APRIL 1987 LIDS-P-1665

Inversion of Parabolic and Paraboloidal Projections[1]

Ali Özbek and Bernard C. Levy[2]

Abstract

The multidimensional inverse scattering problem for an acoustic medium is considered within the homogeneous background Born approximation. A constant density acoustic medium is probed by a wide-band plane wave source, and the scattered field is observed along a receiver array located outside the medium. The inversion problem is formulated as a generalized tomographic problem. It is shown that the observed scattered field can be appropriately filtered so as to obtain generalized projections of the scattering potential. For a 2-D experimental geometry, these projections are weighted integrals of the scattering potential over regions of parabolic support, whereas they become surface integrals over circular paraboloids for the 2-D case. The inversion problem is therefore similar to that of x-ray tomography, except that instead of being given projections of the object to be reconstructed along straight lines, parabolic or paraboloid projections are given. The inversion procedure that we propose is similar to the x-ray solution, in the sense that it consists of a backprojection operation followed by 2- or 3-D space invariant filtering. An alternative interpretation of the backprojection operation in terms of a backpropagated

[1]This work was supported by the Air Force Office of Scientific Research under Grant No. AFOSR-85-0227 and by the National Science Foundation under Grant No. ECS-83-12921.

[2]Laboratory of Information and Decision Systems and Department of Electrical Engineering and Computer Science, Massachusetts Institute of Technology, Cambridge, MA 02139.

field is given. A "Projection-Slice Theorem" is also derived relating the generalized projections and the scattering potential in the Fourier transform domain.

1. Introduction

In inverse scattering problems, the objective is to reconstruct certain physical properties of a medium from scattering experiments. In general, there is an array of sources and an array of receivers located outside the medium. There are three general approaches to the inversion problem: iterative inversion, exact direct inversion and approximate direct inversion. The iterative inversion (also called generalized inversion) approach attempts to solve a very large scale least-squares problem, where at every stage an estimate of the medium parameters is used to solve the forward scattering problem for the corresponding wave field at the receiver locations. Depending on the difference between the observed and the computed scattered waves, a new estimate of the medium model is obtained and the next iteration is performed. These methods are very time consuming, and the convergence of the current methods depends on the accuracy of the initial estimate.

The objective of exact direct inversion methods is to reconstruct the medium properties exactly, with no iterations involved. These methods require a large number of sources and receivers with particular observation geometries which limit their applicability to practical problems. From a theoretical point of view, one-dimensional exact direct inverse scattering methods have reached an advanced level of development (see [3] for an overview), whereas their extension to higher dimensions has proved to be difficult.

Consequently, the logical approach to the practical solution of multidimensional inverse scattering problems is the use of approximate direct inversion methods. The differential equation for wave propagation in a medium can be transformed into the so-called Lippmann-Schwinger integral equation [24]. For example, for an acoustic medium with constant density, this equation expresses in integral form the scattered field inside the medium in terms of the propagation velocity profile and the total pressure field inside the medium. The Born approximation consists of approximating the total field inside the integral representation by the incident field.

Therefore, this approximation assumes that the scattered field is small compared to the incident field; or equivalently that the perturbations of the velocities are small with respect to the background velocity profile which is used to compute the incident field. Another way of interpreting the Born approximation is to view it as a linearization technique, where the relation between the scattered field and the object profile that we want to reconstruct is linear. Physically, the Born approximation takes into account only the singly scattered waves; multiply scattered waves are considered as noise. Note that, depending on the method used to compute the background field, the multiples due to the background model may be included in the scattered field. The multiples due to the residual velocities are neglected.

In this paper, the inverse scattering problem for an acoustic medium is considered within the homogeneous background Born approximation. A constant density acoustic medium is probed by a wide-band plane wave source, and the scattered field is observed along a receiver array located outside the medium. The objective is to reconstruct the scattering potential, which is a function of the propagation velocity inhomogeneities in the medium. The monochromatic plane-wave source inverse scattering problem has been studied under the name of diffraction tomography by several researchers, including Mueller, Kaveh, Devaney and Beylkin [9,10,19]. Roberts and Kak investigated the reflection mode problem with broadband illumination [21], whereas Esmersoy and Levy presented a solution in terms of an extrapolated field [12].

In the present paper, the key observation is that, the time traces observed at the receivers can be appropriately filtered so as to obtain generalized projections of the scattering potential. For a two-dimensional experimental geometry, these projections are weighted integrals of the scattering potential over regions of parabolic support, whereas they become surface integrals over circular paraboloids for the three-dimensional case. Thus the inverse scattering problem is now posed as a generalized tomographic or integral geometric problem.

The straight-line tomography problem, which arises in x-ray tomography, was first solved by Radon [20]; see Deans [8] for a full treatment. Fawcett [13] formulated the zero-offset Born inversion problem as a generalized tomographic problem, where the objective is to reconstruct a function from its projections along circles or spheres.

The reconstruction problem for parabolical projections can be formulated in a way similar to the problem of x-ray tomography. The solution can be expressed as a backprojection operation where we sum the contributions of all projections passing through a given point in space, followed by a two or three dimensional filtering operation.

A different, physically-oriented interpretation of the backprojection operation appearing in our reconstruction technique is developed by showing that it can be obtained by first backpropagating the observed filtered time traces, and then correlating the backpropagated field with the incident probing wave field. A "Projection-Slice Theorem" is also derived relating the generalized projections and the scattering potential in the Fourier transform domain.

The paper is organized as follows: we treat the 2-D case in detail in Sections 2-7, and just summarize the results for the 3-D case in Section 8. In Section 2, the inverse scattering problem is formulated within the Born approximation and related to the problem of inversion of parabolic projections. The backprojection operation is defined and related to the parabolic projections in Section 3. A frequency domain relationship between the backprojected image and the true scattering potential is derived in Section 4, where a "Projection-Slice Theorem" is also presented. In Section 5, the backprojection operation is interpreted in terms of a backpropagated field. The results for the 2-D case are summarized in Section 6 and illustrated with a synthetic data example in Section 7. We summarize the results for the 3-D geometry in Section 8, and Section 9 contains the conclusions of the paper.

2. Problem Description

In this paper we will treat the two-dimensional case in detail, and summarize the results for the three-dimensional case. Consider the scattering experiment described in Fig. 1. A constant density 2-D acoustic medium is probed by a wide-band plane wave and the scattered field is observed along a straight-line receiver array. The Fourier transform $P(\underline{x},\omega)$ of the pressure field at position $\underline{x}=(x,y)$ satisfies

$$[\nabla^2 + k^2 n^2(\underline{x})]P(\underline{x},\omega) = 0, \tag{1}$$

where $k=\omega/c_o$ is the wavenumber, $n(\underline{x}) = c_o/c(\underline{x})$ is the refractive index of the medium, $c(\underline{x})$ is the propagation velocity at point $\underline{x}$ and c_o is the propagation velocity of the background medium. We assume that $n(\underline{x})$ does not deviate significantly from the background index of 1, so that

$$n^2(\underline{x}) = 1 + U(\underline{x}), \tag{2}$$

where the scattering potential $U(\underline{x})$ is small. We also assume that $U(\underline{x})$ has a bounded support V, which is completely located on the same side of the receiver array, as shown in Fig. 1. Decomposing the total field P into the incident field P_o and the scattered field

$$P(\underline{x},\omega) \triangleq P_o(\underline{x},\omega) + P_s(\underline{x},\omega), \tag{3}$$

and noting that the incident field P_o satisfies the Helmholtz equation associated with the background medium:

$$(\nabla^2 + k^2)P_o(\underline{x},\omega) = 0, \tag{4}$$

we find that the scattered field P_s satisfies the equation

$$(\nabla^2 + k^2)P_s(\underline{x},\omega) = -k^2 U(\underline{x})P(\underline{x},\omega). \tag{5}$$

The solution of (5) is given by the Lippmann-Schwinger equation [24]

$$P_s(\underline{x},\omega) = k^2 \int d\underline{x}' U(\underline{x}') P(\underline{x}',\omega) G_o(\underline{x},\underline{x}',\omega), \tag{6}$$

where $G_o(\underline{x},\underline{x}',\omega)$ is the Green's function associated with a point source in a homogeneous medium:

$$(\nabla^2 + k^2) G_o(\underline{x},\underline{x}',\omega) = -\delta(\underline{x}-\underline{x}'). \tag{7}$$

Equation (6) demonstrates the nonlinear relation that exists between the potential $U(\underline{x})$ and the pressure field $P(\underline{x},\omega)$. To linearize this equation we adopt the Born approximation, whereby we assume $P_s(\underline{x},\omega) \ll P_o(\underline{x},\omega)$. Hence the Lippmann-Schwinger equation becomes

$$P_s(\underline{x},\omega) \approx k^2 \int d\underline{x}' U(\underline{x}') P_o(\underline{x}',\omega) G_o(\underline{x},\underline{x}',\omega). \tag{8}$$

For the 2-D problem under consideration, the Green's function and the incident wave are given as

$$G_o(\underline{x},\underline{x}',\omega) = \frac{i}{4} H_0^{(1)}(k|\underline{x}-\underline{x}'|), \tag{9}$$

$$P_o(\underline{x}',\omega) = e^{ik\hat{\underline{\theta}}\cdot\underline{x}'}, \tag{10}$$

where $\hat{\underline{\theta}} = (\cos\theta,\ \sin\theta)$ is the unit vector which indicates the angle of incidence of the plane-wave source, and $H_0^{(1)}(\cdot)$ indicates the Hankel function of order zero and type one. Therefore, the scattered field at a receiver point $\underline{\xi}$ is given by

$$P_s(\underline{\xi},\omega) = \frac{ik^2}{4} \int d\underline{x}' U(\underline{x}') e^{ik\hat{\underline{\theta}}\cdot\underline{x}'} H_0^{(1)}(k|\underline{x}'-\underline{\xi}|), \tag{11}$$

within the Born approximation. In the following, it is assumed that the receivers are located along a straight line perpendicular to the unit vector $\hat{\underline{\phi}} = (\cos\phi,\ \sin\phi)$ and whose distance from the origin in the direction $\hat{\underline{\phi}}$ is p, as shown in Fig. 1. The position of an arbitrary receiver along this line is therefore given by $\underline{\xi} = p\hat{\underline{\phi}} + \xi\hat{\underline{\phi}}^{\perp}$,

where $\hat{\underline{\phi}}^{\perp} = (\sin\phi, -\cos\phi)$ is a unit vector perpendicular to $\hat{\underline{\phi}}$, and ξ is an arbitrary coordinate. Then (11) can be written as

$$\begin{aligned} \frac{2\pi}{k^2} P_s(\underline{\xi}, \omega) &= \frac{i\pi}{2} \int d\underline{x}' U(\underline{x}') e^{ik\hat{\underline{\theta}}\cdot\underline{x}'} H_0^{(1)}(k|\underline{x}' - \underline{\xi}|) \\ &\triangleq \hat{F}(\xi, k). \end{aligned} \tag{12}$$

Define the inverse Fourier transform of $\hat{F}(\xi, k)$ with respect to k as $g(\xi, r)$:

$$g(\xi, r) \triangleq \frac{1}{2\pi} \int_{-\infty}^{\infty} dk \hat{F}(\xi, k) e^{-ikr}. \tag{13}$$

Taking into account the fact that (see [15], p. 731)

$$\mathcal{F}^{-1}\left\{ \frac{i\pi}{2} H_0^{(1)}(ku) \right\} = \frac{1(r-u)}{\sqrt{r^2 - u^2}}, \tag{14}$$

where $1(\cdot)$ is the unit step function, we find that

$$g(\xi, r) = \int d\underline{x}' U(\underline{x}') \frac{1(r - \hat{\underline{\theta}} \cdot \underline{x}' - |\underline{x}' - \underline{\xi}|)}{\sqrt{(r - \hat{\underline{\theta}} \cdot \underline{x}')^2 - |\underline{x}' - \underline{\xi}|^2}}. \tag{15}$$

This identity expresses $g(\xi, r)$ as a weighted integral of the scattering potential $U(\underline{x})$ where the weighting function is nonzero in a region with parabolic support. The parabola satisfies the equation $r = \hat{\underline{\theta}} \cdot \underline{x} - |\underline{x} - \underline{\xi}|$ where r, $\hat{\underline{\theta}}$ and $\underline{\xi}$ are given and $\underline{x}$ varies, as shown in Fig. 2. The directrix of this parabola is the line $\hat{\underline{\theta}} \cdot \underline{x} = r$ which is perpendicular to the direction $\hat{\underline{\theta}}$ of incidence of the probing wave, and its focus is the receiver point $\underline{\xi}$. The weighting function becomes infinite for values of $\underline{x}$ along this parabola, so that the largest contribution to the integral is made by the values of $U(\underline{x})$ which lie along the parabola. In some sense, $g(\xi, r)$ is a projection of $U(\underline{x})$ with respect to a function whose singularities are algebraic and located along a parabola.

It is then interesting to note that the projections $g(\xi, r)$ can be obtained directly from the observed scattered field $P_s(\underline{\xi}, t)$ in time domain also: from (12) and (13),

$$g(\xi, r) = -2\pi c_o \int_0^{r/c_o} d\tau \int_0^{\tau} ds P_s(\underline{\xi}, s). \tag{16}$$

Thus, the projections $g(\xi, r)$ are proportional to the scattered field twice integrated.

Therefore, given the observed scattered field $P_s(\xi, t)$ for ξ along the line array depicted in Fig. 2, and for $-\infty < t < \infty$, it is a straightforward procedure to find the generalized projection $g(\xi, r)$ for $-\infty < \xi < \infty$ and $0 \leq r < \infty$, and in the following it will be assumed that these projections constitute the data that is given by the scattering experiment. From this point of view, the inverse scattering problem can be formulated as follows: given the generalized projections

$$\{g(\xi, r): \ -\infty < \xi < \infty, \ 0 \leq r < \infty\},$$

we want to reconstruct the scattering potential $U(\underline{x})$.

In some sense, the above reconstruction problem is similar to the problem of x-ray tomography, where we are given the projections

$$g(r, \theta) = \int d\underline{x}' U(\underline{x}') \delta(r - \hat{\underline{\theta}} \cdot \underline{x}') \tag{17}$$

of $U(\underline{x})$ along straight lines. It is also analog to the inverse scattering problem considered by Fawcett [13]. There it was shown that the so-called zero-offset inverse scattering geometry, where coincident point sources and receivers are employed, could be reduced to the solution of a generalized tomographic problem where the objective is to reconstruct a function $U(\underline{x})$ from its projections along circles of arbitrary radii centered along a straight line. There exists however an important difference between the problem of x-ray tomography, or the problem considered by Fawcett [13], and the problem that we examine here. In x-ray tomography, the projections of $U(\underline{x})$ are taken with respect to a weighting function which is the distribution $\delta(r - \hat{\underline{\theta}} \cdot \underline{x}')$, whereas the weighting function appearing in (15) is algebraic. Thus, in 2-D the generalized parabolic projection $g(\xi, r)$ is not an integral along a curve but an integral that has nonzero weighting over a whole region of the plane (the inside of the parabola depicted in Fig. 2). This is due to the fact that the wave associated to the 2-D Green's function does not have an impulsive waveform, but has a tail, as indicated by equation (14).

3. The Backprojection Operation

Like the x-ray tomography inversion procedure, or the method proposed by Fawcett [13] for the case of circular projections, the first step of our inversion procedure is to perform a backprojection operation on the projections $g(\xi, r)$. At a given point $\underline{x}$, this operation sums the contributions of the projections $g(\xi, r)$ which correspond to parabolic regions that include the point $\underline{x}$. In this summation, the projection $g(\xi, r)$ is weighted in proportion to the amount that $U(\underline{x})$ has contributed to it according to the forward scattering equation (15). By performing this backprojection operation for every point in the plane, this gives a backprojection approximation, $U_B(\underline{x})$ to $U(\underline{x})$. It is given by

$$U_B(\underline{x}) \triangleq \int_{-\infty}^{\infty} d\xi \int_0^{\infty} dr g(\xi, r) \frac{1(r - \hat{\underline{\theta}} \cdot \underline{x} - |\underline{x} - \underline{\xi}|)}{\sqrt{(r - \hat{\underline{\theta}} \cdot \underline{x})^2 - |\underline{x} - \underline{\xi}|^2}}. \tag{18}$$

Our first objective is to find a frequency domain relationship between $g(\xi, r)$ and $U_B(\underline{x})$. It can be shown that (see Appendix A)

$$\int d\underline{x} \frac{1(r - \hat{\underline{\theta}} \cdot \underline{x} - |\underline{x} - \underline{\xi}|)}{\sqrt{(r - \hat{\underline{\theta}} \cdot \underline{x})^2 - |\underline{x} - \underline{\xi}|^2}} e^{-i\underline{k} \cdot \underline{x}} = \frac{i\pi}{\underline{k} \cdot \hat{\underline{\theta}}} e^{-i[\underline{\kappa} \cdot (p\hat{\underline{\psi}} + \xi \hat{\underline{\psi}}^{\perp}) + k^2 r]/2\underline{k} \cdot \hat{\underline{\theta}}} \tag{19}$$

where $\underline{k} = (k_x, k_y)$, $k = |\underline{k}|$, $\underline{\kappa} = (k_x^2 - k_y^2,\ 2k_x k_y)$, $\hat{\underline{\psi}} = (\cos(\theta + \phi),\ \sin(\theta + \phi))$, and $\hat{\underline{\psi}}^{\perp} = (\sin(\theta + \phi),\ -\cos(\theta + \phi))$. The Fourier transform of $U_B(\underline{x})$ is therefore given by

$$\begin{aligned} \hat{U}_B(\underline{k}) &\triangleq \int d\underline{x} U_B(\underline{x}) e^{-i\underline{k} \cdot \underline{x}} \\ &= \frac{i\pi}{\underline{k} \cdot \hat{\underline{\theta}}} e^{-ip\underline{\kappa} \cdot \hat{\underline{\psi}}/2\underline{k} \cdot \hat{\underline{\theta}}} \hat{\hat{g}} \left(k_\xi = \frac{\underline{\kappa} \cdot \hat{\underline{\psi}}^{\perp}}{2\underline{k} \cdot \hat{\underline{\theta}}},\ k_r = \frac{k^2}{2\underline{k} \cdot \hat{\underline{\theta}}} \right), \end{aligned} \tag{20}$$

where

$$\hat{\hat{g}}(k_\xi, k_r) = \int_{-\infty}^{\infty} d\xi \int_0^{\infty} dr g(\xi, r) e^{-i(k_\xi \xi + k_r r)} \tag{21}$$

is the 2-D Fourier transform of $g(\xi, r)$.

4. Relationship Between $\hat{U}_B(\underline{k})$ and $\hat{U}(\underline{k})$

We first take the Fourier transform of $g(\xi, r)$ with respect to r:

$$\begin{aligned}\hat{g}(\xi, k_r) &= \int_0^\infty dr g(\xi, r) e^{-ik_r r} \\ &= \hat{F}^*(\xi, k_r) \\ &= -\frac{i\pi}{2} \int d\underline{x}' U(\underline{x}') e^{ik_r \hat{\underline{\theta}} \cdot \underline{x}'} H_0^{(2)}(k_r |\underline{x}' - \underline{\xi}|), \end{aligned} \tag{22}$$

from (12), where $\hat{F}^*$ denotes the complex conjugate of $\hat{F}$ and $H_0^{(2)}(\cdot)$ is the Hankel function of order 0 and type 2. Now, taking the Fourier transform with respect to ξ, for $|k_\xi| \leq |k_r|$ we obtain (see Appendix B)

$$\hat{\hat{g}}(k_\xi, k_r) = -\frac{i\pi \mathrm{sgn}(k_r)}{\sqrt{k_r^2 - k_\xi^2}} e^{i\gamma p \mathrm{sgn}(k_r)\sqrt{k_r^2 - k_\xi^2}} \hat{U}(\underline{k} = k_r \hat{\underline{\theta}} + k_\xi \hat{\underline{\phi}}^\perp + \gamma \mathrm{sgn}(k_r)\sqrt{k_r^2 - k_\xi^2}\, \hat{\underline{\phi}}), \tag{23}$$

where

$$\hat{U}(\underline{k}) = \int d\underline{x}' U(\underline{x}') e^{-i\underline{k} \cdot \underline{x}'} \tag{24}$$

is the 2-D Fourier transform of $U(\underline{x})$, and

$$\gamma \triangleq \begin{cases} +1 & \text{if } \underline{x} \cdot \hat{\underline{\phi}} - p > 0 \text{ for all } \underline{x} \in V, \\ -1 & \text{if } \underline{x} \cdot \hat{\underline{\phi}} - p < 0 \text{ for all } \underline{x} \in V. \end{cases}$$

For normal incidence ($\hat{\underline{\theta}} = \hat{\underline{\phi}}$) and fixed k_r, this result corresponds to the formula obtained by Devaney in the context of diffraction tomography [9]. This relationship is similar to the Projection Slice Theorem of straight-line tomography (see [8], Section 6.2). It relates the 1-D Fourier transform of $\hat{g}(\xi, k_r)$ with respect to ξ to a semicircular slice of the 2-D Fourier transform of $U(\underline{x})$. For a fixed k_r, $\hat{\hat{g}}(k_\xi, k_r)$ gives $\hat{U}(\underline{k})$ along a semicircle of radius $|k_r|$ centered at $k_r \hat{\underline{\theta}}$ as shown in Fig. 3. By letting k_r vary, these semicircles span a cone C, which is defined as

$$\begin{aligned} C = \Bigg\{ k_x, k_y : \frac{1}{2}\left(\theta + \phi - \frac{\pi}{2}\right) \leq \tan^{-1}\frac{k_y}{k_x} \leq \frac{1}{2}\left(\theta + \phi + \frac{\pi}{2}\right) \\ \text{or } \frac{1}{2}\left(\theta + \phi + \frac{3\pi}{2}\right) \leq \tan^{-1}\frac{k_y}{k_x} \leq \frac{1}{2}\left(\theta + \phi + \frac{5\pi}{2}\right) \Bigg\} \end{aligned} \tag{25}$$

for $\gamma = +1$. The angular range of this cone is 90^0, as indicated in Fig. 3. For $\gamma = -1$, C is the complement $\bar{C}$ of the above cone. The above analysis shows that the knowledge of the projections $g(\xi, r)$ for $-\infty < \xi < \infty$ and $0 \leq r < \infty$, or equivalently the knowledge of $\hat{\hat{g}}(k_\xi, k_r)$ for all k_ξ and k_r, specifies the 2-D Fourier transform $\hat{U}(\underline{k})$ only over the cone C, i.e. for $\underline{k} \in C$. This indicates immediately that the projections $g(\xi, r)$ over a single line array are not sufficient to reconstruct completely the scattering potential $U(\underline{x})$.

For $|k_\xi| > |k_r|$, from Appendix B we find that $\hat{\hat{g}}(k_\xi, k_r)$ is related to a 2-D bilateral Laplace transform of $U(\underline{x})$:

$$\hat{\hat{g}}(k_\xi, k_r) = \frac{\pi}{\sqrt{k_\xi^2 - k_r^2}} e^{\gamma p \sqrt{k_\xi^2 - k_r^2}} \int d\underline{x}' U(\underline{x}') e^{-[\gamma \sqrt{k_\xi^2 - k_r^2}\, \hat{\underline{\phi}} + i(k_r \hat{\underline{\theta}} + k_\xi \hat{\underline{\phi}}^\perp)] \cdot \underline{x}'}. \tag{26}$$

This term is the part of the filtered scattered field $g(\xi, r)$ observed at the receivers that corresponds to evanescent waves. Although $\hat{\hat{g}}(k_\xi, k_r)$ in this region contains some information about $U(\underline{x})$, $\hat{\hat{g}}(k_\xi, k_r)$ is not directly related to $\hat{U}(\underline{k})$. Furthermore, the numerical inversion of (26) would be unstable, since the numerical inversion of the Laplace transform is an unstable operation. Therefore, in our inversion scheme we only use $\hat{\hat{g}}(k_\xi, k_r)$ for $|k_\xi| \leq |k_r|$.

The inverse formula of (23) is

$$\hat{U}(\underline{k}) = \frac{i\underline{\kappa} \cdot \hat{\underline{\psi}}}{2\pi \underline{k} \cdot \hat{\underline{\theta}}} e^{-ip\underline{\kappa} \cdot \hat{\underline{\psi}}/2\underline{k} \cdot \hat{\underline{\theta}}} \hat{\hat{g}} \left(k_\xi = \frac{\underline{\kappa} \cdot \hat{\underline{\psi}}^\perp}{2\underline{k} \cdot \hat{\underline{\theta}}},\ k_r = \frac{k^2}{2\underline{k} \cdot \hat{\underline{\theta}}} \right), \quad \underline{k} \in C. \tag{27}$$

Combining (20) and (27) gives

$$\hat{U}(\underline{k}) = \frac{\underline{\kappa} \cdot \hat{\underline{\psi}}}{2\pi^2} \hat{U}_B(\underline{k}), \quad \underline{k} \in C. \tag{28}$$

Therefore, $\hat{U}(\underline{k})$ for $\underline{k} \in C$ can be obtained from $\hat{U}_B(\underline{k})$ by a single 2-D filtering operation. This is similar to the "filter of projections" method used in straight-line tomography (see [8], Section 6.5).

By using the generalized parabolical projections $g(\xi, r)$ obtained from a single straight-line array, we obtain the coverage of $\hat{U}(\underline{k})$ over a 90^0 cone. To obtain a more complete coverage, we can use additional receiver arrays or perform several experiments with plane-waves incident from several directions. Consider for example the experimental set up where for a single plane wave experiment, we employ two parallel receiver arrays located on both sides of the domain V. These two arrays yield values of $\gamma = 1, \ -1$ respectively, and consequently they provide a coverage of $\hat{U}(\underline{k})$ over complementary cones. In exploration geophysics, this corresponds approximately to the borehole to borehole experiment geometry, where the receivers are located along two vertical boreholes on both sides of the region of the earth that needs to be imaged. Note however that in practice these vertical boreholes do not extend deep enough inside the earth to provide coverages of $\hat{U}(\underline{k})$ that are truly complementary.

If a single receiver array is employed, an alternative way to obtain a complete coverage of $\hat{U}(\underline{k})$ is to perform several experiments with plane waves incident from different directions. For two plane waves incident from opposite directions $\underline{\hat{\theta}}$ and $\underline{\hat{\theta}}' = -\underline{\hat{\theta}}$, we obtain again a complete coverage of $\hat{U}(\underline{k})$. However in exploration geophysics, we have usually access to only one side of the medium, namely the surface of the earth, and the above scheme cannot really be used. We are therefore confronted with the situation where only an incomplete coverage of the Fourier transform $\hat{U}(\underline{k})$ is available. A partial reconstruction of $U(\underline{x})$ can then be obtained by setting the missing values of $\hat{U}(\underline{k})$ equal to zero, and by taking the inverse Fourier transform of the resulting function. Needless to say, the reconstructed scattering potential has a number of artifacts. An alternative scheme, which was proposed by Kaveh, Soumekh, and Greenleaf [16,22] in the context of x-ray and diffraction tomography, consists of interpolating the known values of $\hat{U}(\underline{k})$ to obtain the missing values. However, this scheme is computationally more demanding, and in the numerical example of Section 7 below, we will use the simpler scheme where

the missing values of $\hat{U}(\underline{k})$ are set equal to zero.

5. Interpretation of $U_B(\underline{x})$ in Terms of a Backpropagated Field

In this section we provide an interpretation of the backprojected image $U_B(\underline{x})$ based on the concept of a backpropagated field. Backpropagation is an operation in which the wave equation is run backwards in time, using the recorded traces (or filtered versions of them) as source wavelets. In exploration geophysics, where the objective is to image the discontinuities in the velocity profile, this operation is called migration [4,5,7,14]. The difference between migration and inversion methods such as the one that we consider here is that, in migration the objective is to detect only the discontinuities of $U(\underline{x})$, whereas inversion procedures seek to obtain precise quantitative information about the values of the function $U(\underline{x})$ or of its Fourier transform.

Given some receiver observations$P_s(\underline{\xi}, t)$, there are two ways of defining a backpropagated field $P_e(\underline{x}, t)$:

1) We can impose the boundary condition $P_e(\underline{\xi}, t) = P_s(\underline{\xi}, t)$ for all t and receiver locations $\underline{\xi}$, and then use a finite difference implementation of the wave equation to propagate the extrapolated field P_e backwards in time inside the domain V. This is the choice made by Esmersoy and his colleagues [10,11].

2) We can replace each receiver $\underline{\xi}$ by a source and select as source wavelet at $\underline{\xi}$ a function $S(\xi, k)$ of the observed scattered field. This is the choice we make here. Defining the source wavelet as

$$S(\xi, k) = 2\pi \hat{F}(\xi, k) = \frac{4\pi^2}{k^2} P_s(\underline{\xi}, k), \tag{29}$$

the extrapolated field is

$$P_e(\underline{x}, k) = \int_{-\infty}^{\infty} d\xi S(\xi, k) \left[-\frac{i}{4} H_0^{(2)}(k|\underline{x} - \underline{\xi}|) \right], \tag{30}$$

where the Green's function $-\frac{i}{4}H_0^{(2)}(k|\underline{x}-\underline{\xi}|)$ must be used because the field is propagated backwards in time. In the time domain, (30) becomes

$$P_e(\underline{x},t) = \int_{-\infty}^{\infty} d\xi g(\xi,t) * G_o^{(2)}(\underline{x},\underline{\xi},t), \tag{31}$$

where $*$ denotes the convolution operation with respect to time,

$$g(\xi,t) = \mathcal{F}^{-1}[\hat{F}(\xi,k)], \tag{32}$$

$$\begin{aligned} G_o^{(2)}(\underline{x},\underline{\xi},t) &\triangleq \mathcal{F}^{-1}\left\{-\frac{i\pi}{2}H_0^{(2)}(k|\underline{x}-\underline{\xi}|)\right\} \\ &= \frac{1(-t-|\underline{x}-\underline{\xi}|)}{\sqrt{t^2-|\underline{x}-\underline{\xi}|^2}}, \end{aligned} \tag{33}$$

and

$$g(\xi,t) * G_o^{(2)}(\underline{x},\underline{\xi},t) = \int_0^{\infty} dr g(\xi,r)\frac{1(-(t-r)-|\underline{x}-\underline{\xi}|)}{\sqrt{(t-r)^2-|\underline{x}-\underline{\xi}|^2}}. \tag{34}$$

If we now image the backpropagated field at the source travel times $\tau(\underline{x}) = \hat{\underline{\theta}}\cdot\underline{x}$, where $\tau(\underline{x})$ represents the time at which the incident plane wavefront reaches point $\underline{x}$, we obtain

$$\begin{aligned} P_e(\underline{x},\tau(\underline{x})) &= \int_{-\infty}^{\infty} d\xi \int_0^{\infty} dr g(\xi,r)\frac{1(r-\hat{\underline{\theta}}\cdot\underline{x}-|\underline{x}-\underline{\xi}|)}{\sqrt{(r-\hat{\underline{\theta}}\cdot\underline{x})^2-|\underline{x}-\underline{\xi}|^2}} \\ &= U_B(\underline{x}). \end{aligned} \tag{35}$$

Note that the choice of source travel times as imaging rule comes from the time correlation

$$\begin{aligned} &\int_0^{\infty} dt P_o(\underline{x},t)P_e(\underline{x},t) \\ &= \int_0^{\infty} dt\delta(t-\hat{\underline{\theta}}\cdot\underline{x})P_e(\underline{x},t) \\ &= P_e(\underline{x},\tau(\underline{x})), \end{aligned} \tag{36}$$

where $P_o(\underline{x},t) = \delta(t - \hat{\underline{\theta}} \cdot \underline{x})$ is the incident field.

Thus the backpropagated image $U_B(\underline{x})$ can be viewed as obtained by

1) Backpropagating the observed scattered field,

2) Imaging at the source travel times.

Correlation of the backpropagated field with the incident field, or equivalently, imaging the backpropagated field at source travel times is an imaging rule that is encountered in a variety of inversion methods. Chang and McMechan [6] have developed a migration technique based on this principle, while Tarantola [23] has shown that the update operations in an iterative inversion algorithm can be written in terms of this correlation operation.

6. Summary of the Results for 2-D Geometry

Once $U_B(\underline{k})$ is found, $U(\underline{x})$ can be reconstructed by inverse Fourier transforming

$$\hat{U}(\underline{k}) = \begin{cases} (\underline{\kappa} \cdot \hat{\underline{\psi}}/2\pi^2)\hat{U}_B(\underline{k}), & \underline{k} \in C, \\ 0, & \underline{k} \in \bar{C}. \end{cases} \tag{37}$$

$U_B(\underline{k})$ can be computed two ways:

Method 1:

1. Compute the generalized parabolical projections as

$$g(\xi, r) = -2\pi c_o \int_0^{r/c_o} d\tau \int_0^{\tau} ds P_s(\underline{\xi}, s), \tag{38}$$

or

$$\hat{g}(\xi, k_r) = \frac{2\pi}{k_r{}^2} P_s(\underline{\xi}, c_o k_r). \tag{39}$$

2. Then

$$\hat{U}_B(\underline{k}) = \frac{i\pi}{\underline{k} \cdot \hat{\underline{\theta}}} e^{-ip\underline{\kappa} \cdot \hat{\underline{\psi}}/2\underline{k} \cdot \hat{\underline{\theta}}} \hat{\hat{g}}\left(k_\xi = \frac{\underline{\kappa} \cdot \hat{\underline{\psi}}^{\perp}}{2\underline{k} \cdot \hat{\underline{\theta}}}, k_r = \frac{k^2}{2\underline{k} \cdot \hat{\underline{\theta}}} \right), \tag{40}$$

where $\hat{\hat{g}}(k_\xi, k_r)$ is the 2-D Fourier transform of $g(\xi, r)$.

Method 2:

1. Compute the backpropagation source wavelet:

$$S(\xi, k) = \frac{4\pi^2}{k^2} P_s(\underline{\xi}, k). \tag{41}$$

2. Compute the extrapolated field

$$P_e(\underline{x}, k) = \int_{-\infty}^{\infty} d\xi S(\xi, k) \left[-\frac{i}{4} H_0^{(2)}(k|\underline{x} - \underline{\xi}|) \right]. \tag{42}$$

3. Inverse Fourier transform $P_e(\underline{x}, k)$:

$$P_e(\underline{x}, \tau) = \mathcal{F}^{-1}[P_e(\underline{x}, k)]. \tag{43}$$

4. Image the extrapolated field at the source travel time $\tau(\underline{x}) = \hat{\underline{\theta}} \cdot \underline{x}$. This gives

$$U_B(\underline{x}) = P_e(\underline{x}, \hat{\underline{\theta}} \cdot \underline{x}). \tag{44}$$

5. Fourier transforming $U_B(\underline{x})$ gives $\hat{U}_B(\underline{k})$.

7. Numerical Example

We present computer simulation results corresponding to a simple example. Fig. 4 shows the scattering potential to be reconstructed. It represents a $\pm 5\%$ variation in the propagation velocity with respect to the constant background velocity. In the experiments that we consider, the probing plane-wave was sent perpendicularly to Side A and receivers were placed on all four sides of the domain where the scattering potential is located. The scattered waves were computed by a finite-difference algorithm. The source wavelet used was a Blackman-Harris window and the diameter of the object was twice the dominant wavelength contained in the probing wavelet. Fig. 5 shows the reconstruction obtained using only the receivers

on Side A, while Figs. 6 and 7 show the same for the cases where the receivers are only located on Sides B and C respectively. Fig. 8 depicts the reconstruction using all the receivers.

Figs. 9, 10 and 11 show the frequency domain coverage theoretically obtained by using infinite receiver arrays located on sides A, B, and C, respectively. The lightly shaded regions indicate the coverage for the case of an infinite bandwidth source, whereas the darkly shaded regions mark the coverage for a finite bandwidth source, such as the one that was used here. The actual coverage obtained in the above experiment was less than the one which is shown in these diagrams since the receiver arrays have only a finite size, instead of being infinite, as was assumed in Figs. 9-11. For finite arrays the coverage obtained at any particular point of reconstruction varies according to its position with respect to the array.

8. Three-Dimensional Geometry

After discussing the 2-D experimental geometry, we summarize the corresponding results for the 3-D case. For the 3-D geometry, we assume that the receivers are on a plane; for convenience we choose this to be the x-y plane. The position of an arbitrary receiver located in this plane is therefore given by $\underline{\xi} = (\underline{\xi}_T, 0)$, where $\underline{\xi}_T$ represents the x-y coordinates of the receiver. The Green's function due to a point source is

$$G_o(\underline{x}, \underline{x}', \omega) = \frac{e^{ik|\underline{x} - \underline{x}'|}}{4\pi|\underline{x} - \underline{x}'|}. \tag{45}$$

Under the Born approximation, the Lippmann-Schwinger equation takes the form (8), and the projections in this case become

$$\begin{aligned} g(\underline{\xi}_T, r) &= \frac{1}{2\pi}\int_{-\infty}^{\infty} dk \left\{\frac{4\pi}{k^2} P_s(\underline{\xi}, \omega)\right\} e^{-ikr} \\ &= \int d\underline{x}' U(\underline{x}') \frac{\delta(r - \hat{\underline{\theta}} \cdot \underline{x}' - |\underline{x}' - \underline{\xi}|)}{|\underline{x}' - \underline{\xi}|}, \end{aligned} \tag{46}$$

where $\underline{\hat{\theta}}$ is again the unit vector in the direction of propagation of the incident wave. Therefore, the projection $g(\underline{\xi}_T, r)$ is a surface integral of the scattering potential over a circular paraboloid. The weighting function appearing in the representation (46) of $g(\underline{\xi}_T, r)$ is an impulse, and in this sense the 3-D case is quite different from the 2-D case.

From (46), in the time domain we can write

$$g(\underline{\xi}_T, r) = -4\pi c_o \int_0^{r/c_o} d\tau \int_0^{\tau} ds P_s(\underline{\xi}, s). \tag{47}$$

Like in the 2-D case, the projections $g(\underline{\xi}_T, r)$ are proportional to the scattered field twice integrated.

The backprojection operation can be defined as before:

$$U_B(\underline{x}) \triangleq \int d\underline{\xi}_T \int_0^{\infty} dr g(\underline{\xi}_T, r) \frac{\delta(r - \underline{\hat{\theta}} \cdot \underline{x} - |\underline{x} - \underline{\xi}|)}{|\underline{x} - \underline{\xi}|}. \tag{48}$$

In the frequency domain, the backprojected image can be related to the parabolical projections as (see Appendix C)

$$\hat{U}_B(\underline{k}) = \frac{i2\pi}{\underline{k} \cdot \underline{\hat{\theta}}} \hat{\hat{g}}\left(\underline{k}_{\xi T} = \left(\frac{\underline{\kappa}_x \cdot \underline{\hat{\theta}}}{2\underline{k} \cdot \underline{\hat{\theta}}}, \frac{\underline{\kappa}_y \cdot \underline{\hat{\theta}}}{2\underline{k} \cdot \underline{\hat{\theta}}}\right), \; k_r = \frac{k^2}{2\underline{k} \cdot \underline{\hat{\theta}}}\right), \tag{49}$$

where

$$\hat{U}_B(\underline{k}) \triangleq \int d\underline{x} U_B(\underline{x}) e^{-i\underline{k} \cdot \underline{x}} \tag{50}$$

$$\hat{\hat{g}}(\underline{k}_{\xi T}, k_r) \triangleq \int d\underline{\xi}_T \int_0^{\infty} dr g(\underline{\xi}_T, r) e^{-i(\underline{k}_{\xi T} \cdot \underline{\xi}_T + k_r r)}, \tag{51}$$

are the 3-D Fourier transforms of $U_B(\underline{x})$ and $g(\underline{\xi}_T, r)$, and

$$\underline{\kappa}_x \triangleq (k_x^2 - k_y^2 - k_z^2, \; 2k_x k_y, \; 2k_x k_z),$$
$$\underline{\kappa}_y \triangleq (2k_x k_y, \; k_y^2 - k_x^2 - k_z^2, \; 2k_y k_z).$$

The projections can also be related to the scattering potential $U(\underline{x})$ by using the forward scattering equation, as shown in Appendix D. For $|\underline{k}_{\xi T}| \leq |k_r|$, this gives

$$\hat{\hat{g}}(\underline{k}_{\xi T}, k_r) = -\frac{i2\pi \mathrm{sgn}(k_r)}{\sqrt{k_r^2 - |\underline{k}_{\xi T}|^2}} \hat{U}(\underline{k} = k_r \underline{\hat{\theta}} + (\underline{k}_{\xi T}, \gamma \mathrm{sgn}(k_r) \sqrt{k_r^2 - |\underline{k}_{\xi T}|^2})), \tag{52}$$

where $\hat{U}(\underline{k})$ is the 3-D Fourier transform of $U(\underline{x})$, and

$$\gamma \triangleq \begin{cases} +1 & \text{if } z > 0 \text{ for all } \underline{x} \in V, \\ -1 & \text{if } z < 0 \text{ for all } \underline{x} \in V. \end{cases}$$

For $|\underline{k}_{\xi T}| > |k_r|$, as in the 2-D case, $\hat{\hat{g}}(\underline{k}_{\xi T}, k_r)$ is related to the part of the observed scattered field that corresponds to evanescent waves, and we do not make use of this portion of $\hat{\hat{g}}(\underline{k}_{\xi T}, k_r)$ in our inversion scheme.

This result represents the "Projection Slice Theorem" for the 3-D case. For a fixed k_r, the 2-D Fourier transform of $\hat{g}(\underline{\xi}_T, k_r)$ gives the 3-D Fourier transform of $U(\underline{x})$ over a hemisphere of radius $|k_r|$ centered at $k_r\underline{\hat{\theta}}$. By letting k_r vary, $\hat{U}(\underline{k})$ is determined in a cone C, which again covers half of the 3-D frequency space.

The inverse formula of (52) is

$$\hat{U}(\underline{k}) = \frac{i\underline{\kappa}_z \cdot \underline{\hat{\theta}}}{4\pi \underline{k} \cdot \underline{\hat{\theta}}} \hat{\hat{g}}\left(\underline{k}_{\xi T} = \left(\frac{\underline{\kappa}_x \cdot \underline{\hat{\theta}}}{2\underline{k} \cdot \underline{\hat{\theta}}}, \frac{\underline{\kappa}_y \cdot \underline{\hat{\theta}}}{2\underline{k} \cdot \underline{\hat{\theta}}} \right), \; k_r = \frac{k^2}{2\underline{k} \cdot \underline{\hat{\theta}}} \right), \quad \underline{k} \in C, \tag{53}$$

where

$$\underline{\kappa}_z \triangleq (2k_x k_z, \; 2k_y k_z, \; k_z^2 - k_x^2 - k_y^2).$$

Combining (49) and (53) gives

$$\hat{U}(\underline{k}) = \frac{\underline{\kappa}_z \cdot \underline{\hat{\theta}}}{8\pi^2} \hat{U}_B(\underline{k}), \quad \underline{k} \in C. \tag{54}$$

Therefore, $\hat{U}(\underline{k})$ for $\underline{k} \in C$ can be obtained from $\hat{U}_B(\underline{k})$ by a 3-D space invariant filtering operation. By using the paraboloidal projections obtained from a single plane array, we obtain the coverage of $\hat{U}(\underline{k})$ over a cone of 2π steradians. Again the coverage can be increased by conducting additional scattering experiments with different geometries.

It is also possible in the 3-D case to give an interpretation of $U_B(\underline{x})$ in terms of a backpropagated field. Replacing each receiver by a source and defining the source wavelet as

$$S(\underline{\xi}_T, k) = \frac{16\pi^2}{k^2} P_s(\underline{\xi}, \omega), \tag{55}$$

the extrapolated field can be defined as

$$P_e(\underline{x},k) = \int d\underline{\xi}_T S(\underline{\xi}_T,k)\frac{e^{-ik|\underline{x}-\underline{\xi}|}}{4\pi|\underline{x}-\underline{\xi}|}, \tag{56}$$

where again the complex conjugate of the Green's function is used, since the field is propagated backwards in time. In the time domain, (56) corresponds to

$$P_e(\underline{x},t) = \int d\underline{\xi}_T g(\underline{\xi}_T,t) * \frac{\delta(-t-|\underline{x}-\underline{\xi}|)}{|\underline{x}-\underline{\xi}|}. \tag{57}$$

Correlating this backpropagated field with the incident field $P_o(\underline{x},t) = \delta(t-\hat{\underline{\theta}}\cdot\underline{x})$, we have

$$\begin{aligned} & \int_{-\infty}^{\infty} dt P_o(\underline{x},t)P_e(\underline{x},t) \\ = & \int d\underline{\xi}_T \int_0^{\infty} dr g(\underline{\xi}_T,r)\frac{\delta(r-\hat{\underline{\theta}}\cdot\underline{x}-|\underline{x}-\underline{\xi}|}{|\underline{x}-\underline{\xi}|} \\ = & U_B(\underline{x}). \end{aligned} \tag{58}$$

9. Conclusion

In this paper we have considered the direct velocity inversion problem for a constant-density acoustic medium probed by a single wide-band plane wave. The problem was posed as a generalized tomographic problem, where weighted integrals of the scattering potential $U(\underline{x})$ over parabolic or paraboloidal regions are considered as data. Drawing analogy to x-ray tomography, a backprojection operator, $U_B(\underline{x})$ was defined, which can be viewed as a "migration" approximation to $U(\underline{x})$. $U_B(\underline{x})$ was related to the generalized projections in the Fourier transform domain. The parabolical projections were also related to $U(\underline{x})$ in the frequency domain, thus deriving a "Projection Slice Theorem". Finally, an interpretation of $U_B(\underline{x})$ was given in terms of a backpropagated field.

In this paper, a constant background Born approximation was used, and within this approximation, the inversion problem was solved exactly. A solution of the

variable background Born inversion problem was presented by Beylkin, Miller and Oristaglio [2,17], who formulated this problem as a generalized Radon transform (GRT) inversion problem, where the objective is to reconstruct a function from its projections along a set of curves whose geometry depends on the experiment and on the background model. In addition to the Born approximation, their solution relies on high frequency asymptotics, and an additional approximation which have the combined effect that the reconstructed potential recovers only the high wavenumber part of the Fourier transform of the true potential. It is interesting to note that, while the inverse GRT method is more general since it can accommodate a variable background, it does not reduce to our solution for a constant background. Therefore the two methods are in a sense complementary, as a tradeoff exists between the generality of the assumptions and the exactness of the solution based on these assumptions.

Acknowledgements

The numerical example in this paper was prepared while the first author was a summer student at Schlumberger-Doll Research. He especially wishes to thank Dr. Cengiz Esmersoy and Dr. Douglas Miller for their assistance.

Appendix A

Derivation of equation (19).

We first compute the Fourier transform

$$F_0(\underline{k},r)\triangleq\int d\underline{x}e^{-i\underline{k}\cdot\underline{x}}\frac{1(r-y-|\underline{x}|)}{\sqrt{(r-y)^2-|\underline{x}|^2}}. \tag{A.1}$$

where $\underline{x}$ is a point with coordinates (x,y). Using the properties of the unit step function, we have

$$F_0(\underline{k},r)=\frac{1}{\sqrt{2r}}\int_{-\infty}^{\infty}dxe^{-ik_xx}\int_{-\infty}^{y_o}dy\frac{e^{-ik_yy}}{\sqrt{y_o-y}}, \tag{A.2}$$

where $y_o=(r^2-x^2)/2r$. With the change of variables $v=y_o-y$,

$$F_0(\underline{k},r)=\frac{e^{-ik_yr/2}}{\sqrt{2r}}G(k_y)M(k_x,k_y,r), \tag{A.3}$$

where ([15], p. 418)

$$G(k_y)=\int_0^{\infty}dv\frac{e^{ik_yv}}{\sqrt{v}}=\sqrt{\frac{\pi}{|k_y|}}e^{i\frac{\pi}{4}\mathrm{sgn}(k_y)}, \tag{A.4}$$

and

$$M(k_x,k_y,r)=\int_{-\infty}^{\infty}dxe^{i[(k_y/2r)x^2-k_xx]}. \tag{A.5}$$

We have

$$\frac{k_y}{2r}x^2-k_xx=\mathrm{sgn}(k_y)\left\{\sqrt{\frac{|k_y|}{2r}}x-\frac{k_x}{2}\sqrt{\frac{2r}{|k_y|}}\mathrm{sgn}(k_y)\right\}^2-\frac{k_x^2r}{2k_y}, \tag{A.6}$$

so that for the change of variables

$$u=\sqrt{\frac{|k_y|}{2r}}x-\frac{k_x}{2}\sqrt{\frac{2r}{|k_y|}}\mathrm{sgn}(k_y),$$

we obtain

$$M(k_x, k_y, r) = e^{-i(k_x^2/2k_y)r}\sqrt{\frac{2r}{|k_y|}}\int_{-\infty}^{\infty} du e^{iu^2 \mathrm{sgn}(k_y)}. \tag{A.7}$$

But ([15], p. 395)

$$\int_{-\infty}^{\infty} du e^{iu^2 \mathrm{sgn}(k_y)} = \sqrt{\pi} e^{i\frac{\pi}{4}\mathrm{sgn}(k_y)}, \tag{A.8}$$

giving

$$M(k_x, k_y, r) = \sqrt{\frac{2\pi r}{|k_y|}}\, e^{-i\left[\frac{k_x^2}{2k_y}r - \frac{\pi}{4}\mathrm{sgn}(k_y)\right]}. \tag{A.9}$$

Combining (A.3), (A.4) and (A.9) yields

$$F_0(\underline{k}, r) = \frac{i\pi}{k_y}\, e^{-i\frac{k^2}{2k_y}r}, \tag{A.10}$$

where $k = |\underline{k}|$.

Now, we compute the Fourier transform

$$F_1(\underline{k}, r, \hat{\underline{\theta}}) \triangleq \int d\underline{x} e^{-i\underline{k}\cdot\underline{x}} \frac{1(r - \hat{\underline{\theta}}\cdot\underline{x} - |\underline{x}|)}{\sqrt{(r - \hat{\underline{\theta}}\cdot\underline{x})^2 - |\underline{x}|^2}}. \tag{A.11}$$

Define the change of variables $\underline{u} = \Theta\underline{x}$, where Θ is a rotation by an angle $\theta - \frac{\pi}{2}$ which aligns the vector $\hat{\underline{\theta}}$ with the y axis. Θ can be represented as $\Theta = (\hat{\underline{\theta}}^{\perp\prime}\hat{\underline{\theta}}')'$ where $\hat{\underline{\theta}}^{\perp} = (\sin\theta, -\cos\theta)$ is a unit vector perpendicular to $\hat{\underline{\theta}}$, and we have

$$\begin{aligned} F_1(\underline{k}, r, \hat{\underline{\theta}}) &= F_0(\Theta\underline{k}, r) \\ &= \frac{i\pi}{\underline{k}\cdot\hat{\underline{\theta}}}\, e^{-i\frac{k^2}{2\underline{k}\cdot\hat{\underline{\theta}}}r}. \end{aligned} \tag{A.12}$$

Next, consider the Fourier transform

$$F_2(\underline{k}, r, \hat{\underline{\theta}}, \underline{\xi}) \triangleq \int d\underline{x} e^{-i\underline{k}\cdot\underline{x}} \frac{1(r - \hat{\underline{\theta}}\cdot\underline{x} - |\underline{x} - \underline{\xi}|)}{\sqrt{(r - \hat{\underline{\theta}}\cdot\underline{x})^2 - |\underline{x} - \underline{\xi}|^2}}. \tag{A.13}$$

Employing the change of variables $\underline{u} = \underline{x} - \underline{\xi}$, we get

$$\begin{aligned} F_2(\underline{k}, r, \hat{\underline{\theta}}, \underline{\xi}) &= e^{-i\underline{k}\cdot\underline{\xi}} \int d\underline{u} e^{-i\underline{k}\cdot\underline{u}} \frac{1[(r - \hat{\underline{\theta}}\cdot\underline{\xi}) - \hat{\underline{\theta}}\cdot\underline{u} - |\underline{u}|]}{\sqrt{[(r - \hat{\underline{\theta}}\cdot\underline{\xi}) - \hat{\underline{\theta}}\cdot\underline{u}]^2 - |\underline{u}|^2}} \\ &= e^{-i\underline{k}\cdot\underline{\xi}} F_1(\underline{k}, r - \hat{\underline{\theta}}\cdot\underline{\xi}, \hat{\underline{\theta}}). \end{aligned} \tag{A.14}$$

Evaluating $F_2(\underline{k}, r, \hat{\underline{\theta}}, \underline{\xi})$ for $\underline{\xi} = p\hat{\underline{\phi}} + \xi\hat{\underline{\phi}}^{\perp}$ and rearranging terms, we obtain (19).

Appendix B

Derivation of equations (23) and (26).

From (22), we have

$$\begin{aligned}\hat{\hat{g}}(k_\xi, k_r) &= \int_{-\infty}^{\infty} d\xi e^{-ik_\xi \xi} \hat{g}(\xi, k_r) \\ &= -\frac{i\pi}{2} \int d\underline{x}' U(\underline{x}') e^{-ik_r \hat{\underline{\theta}} \cdot \underline{x}'} N(\underline{x}', k_\xi, k_r), \end{aligned} \tag{B.1}$$

where

$$N(\underline{x}', k_\xi, k_r) = \int_{-\infty}^{\infty} d\xi e^{-ik_\xi \xi} H_0^{(2)}(k_r |\underline{x}' - \underline{\xi}|). \tag{B.2}$$

We now compute $N(\underline{x}', k_\xi, k_r)$. We can write

$$\begin{aligned} N(\underline{x}', k_\xi, k_r) &= \int_{-\infty}^{\infty} d\xi e^{-ik_\xi \xi} H_0^{(2)} \left\{ k_r |\underline{x}' - (p\hat{\underline{\phi}} + \xi\hat{\underline{\phi}}^{\perp})| \right\} \\ &= \int_{-\infty}^{\infty} d\xi e^{-ik_\xi \xi} H_0^{(2)} \left\{ k_r \sqrt{(\xi - \underline{x}' \cdot \hat{\underline{\phi}}^{\perp})^2 + (p - \underline{x}' \cdot \hat{\underline{\phi}})^2} \right\}. \end{aligned} \tag{B.3}$$

Introducing the change of variables $\eta = \xi - \underline{x}' \cdot \hat{\underline{\phi}}^{\perp}$, we write

$$N(\underline{x}', k_\xi, k_r) = e^{-ik_\xi \underline{x}' \cdot \hat{\underline{\phi}}^{\perp}} \int_{-\infty}^{\infty} d\eta e^{-ik_\xi \eta} H_0^{(2)} \left\{ k_r \sqrt{\eta^2 + (p - \underline{x}' \cdot \hat{\underline{\phi}})^2} \right\}, \tag{B.4}$$

and use the following representation for $H_0^{(2)}(\cdot)$, which corresponds to the Weyl integral decomposition of a circular wave into plane waves ([18], p. 823)

$$H_0^{(2)} \left\{ k_r \sqrt{\eta^2 + (p - \underline{x}' \cdot \hat{\underline{\phi}})^2} \right\} = \frac{\mathrm{sgn}(k_r)}{\pi} \int_{-\infty}^{\infty} d\mu \, \frac{e^{-i\mathrm{sgn}(k_r)(\mu\eta + \sqrt{k_r^2 - \mu^2}|p - \underline{x}' \cdot \hat{\underline{\phi}}|)}}{\sqrt{k_r^2 - \mu^2}}, \tag{B.5}$$

so that in this case

$$N(\underline{x}', k_\xi, k_r) = \frac{2\mathrm{sgn}(k_r)}{\sqrt{k_r^2 - k_\xi^2}} e^{-i(k_\xi \underline{x}' \cdot \hat{\underline{\phi}}^{\perp} + \mathrm{sgn}(k_r)\sqrt{k_r^2 - k_\xi^2}|p - \underline{x}' \cdot \hat{\underline{\phi}}|)}, \quad \text{for } |k_\xi| \leq |k_r|, \tag{B.6}$$

and

$$N(\underline{x}', k_\xi, k_r) = \frac{2}{-i\sqrt{k_\xi^2 - k_r^2}} e^{-ik_\xi \underline{x}' \cdot \hat{\underline{\phi}}^\perp} e^{-\sqrt{k_\xi^2 - k_r^2}|p - \underline{x}' \cdot \hat{\underline{\phi}}|}, \quad \text{for } |k_\xi| > |k_r|, \tag{B.7}$$

where we have recognized that

$$\int_{-\infty}^{\infty} d\eta e^{-i(k_\xi + \mu)\eta} = 2\pi\delta(\mu + k_\xi). \tag{B.8}$$

Substituting (B.6) and (B.7) into (B.1) gives (23) and (26), respectively.

Appendix C

Derivation of equation (49).

We first compute the Fourier transform

$$F_0(\underline{k}, r) \triangleq \int d\underline{x} e^{-i\underline{k}\cdot\underline{x}} \frac{\delta(r - z - |\underline{x}|)}{|\underline{x}|}. \tag{C.1}$$

where $\underline{x}$ is a 3-D point with coordinates (x, y, z). In the following we denote respectively by $\underline{x}_T$ and $\underline{k}_T$ the projections of $\underline{x}$ and $\underline{k}$ onto the x-y plane. Using the cylindrical coordinates $\underline{x} = (\underline{x}_T, z) = (\rho, \alpha, z)$ and $\underline{k} = (\underline{k}_T, k_z) = (k_T, \beta, k_z)$, we obtain

$$F_0(\underline{k}, r) = 2\pi \int_0^\infty d\rho\rho J_0(k_T\rho) \int_{-\infty}^{\infty} dz e^{-ik_z z} \frac{\delta(r - z - \sqrt{\rho^2 + z^2})}{\sqrt{\rho^2 + z^2}}, \tag{C.2}$$

where we have made the identification

$$\int_0^{2\pi} d\alpha e^{-ik_T\rho\cos(\alpha - \beta)} = 2\pi J_0(k_T\rho), \tag{C.3}$$

for arbitrary β. Here, $J_0(\cdot)$ is the Bessel function of order 0 and type 1. Evaluating the integral over z in (C.2), we get

$$F_0(\underline{k}, r) = \frac{2\pi}{r} e^{-ik_z r/2} \int_0^\infty d\rho\rho J_0(k_T\rho) e^{i\frac{k_z}{2r}\rho^2}; \tag{C.4}$$

and by noting that ([15], p. 758)

$$\int_0^\infty d\rho\rho J_0(b\rho)e^{ia\rho^2} = \frac{i}{2a}e^{-ib^2/4a}, \tag{C.5}$$

we find

$$F_0(\underline{k}, r) = \frac{i2\pi}{k_z}e^{-i\frac{k^2}{2k_z}r}, \tag{C.6}$$

where $k = |\underline{k}| = \sqrt{k_T^2 + k_z^2}$.

Now, we compute the Fourier transform

$$F_1(\underline{k}, r, \hat{\underline{\theta}}) \triangleq \int d\underline{x} e^{-i\underline{k}\cdot\underline{x}} \frac{\delta(r - \hat{\underline{\theta}}\cdot\underline{x} - |\underline{x}|)}{|\underline{x}|}. \tag{C.7}$$

Defining the change of variables $\underline{u} = \Theta\underline{x}$, where Θ is again a rotation which aligns the $\hat{\underline{\theta}}$ vector with the z axis, we have

$$\begin{aligned} F_1(\underline{k}, r, \hat{\underline{\theta}}) &= F_0(\Theta\underline{k}, r) \\ &= \frac{i2\pi}{\underline{k}\cdot\hat{\underline{\theta}}} e^{-i\frac{k^2}{2\underline{k}\cdot\hat{\underline{\theta}}}r}. \end{aligned} \tag{C.8}$$

Next, consider the Fourier transform

$$F_2(\underline{k}, r, \hat{\underline{\theta}}, \underline{\xi}) \triangleq \int d\underline{x} e^{-i\underline{k}\cdot\underline{x}} \frac{\delta(r - \hat{\underline{\theta}}\cdot\underline{x} - |\underline{x} - \underline{\xi}|)}{|\underline{x} - \underline{\xi}|}, \tag{C.9}$$

where $\underline{\xi} = (\underline{\xi}_T, 0)$. Using the change of variables $\underline{u} = \underline{x} - \underline{\xi}$, we get

$$F_2(\underline{k}, r, \hat{\underline{\theta}}, \underline{\xi}) = e^{-i\underline{k}_T\cdot\underline{\xi}_T} F_1(\underline{k}, r - \hat{\underline{\theta}}\cdot\underline{\xi}, \hat{\underline{\theta}}). \tag{C.10}$$

Rearranging terms, we obtain

$$F_2(\underline{k}, r, \hat{\underline{\theta}}, \underline{\xi}) = \frac{i2\pi}{\underline{k}\cdot\hat{\underline{\theta}}} e^{-i[(\underline{\kappa}_x\cdot\hat{\underline{\theta}}, \underline{\kappa}_y\cdot\hat{\underline{\theta}})\cdot\underline{\xi}_T + k^2 r]/2\underline{k}\cdot\hat{\underline{\theta}}}, \tag{C.11}$$

where

$$\begin{aligned} \underline{\kappa}_x &\triangleq (k_x^2 - k_y^2 - k_z^2,\ 2k_xk_y,\ 2k_xk_z), \\ \underline{\kappa}_y &\triangleq (2k_xk_y,\ k_y^2 - k_x^2 - k_z^2,\ 2k_yk_z). \end{aligned}$$

From (48), taking the Fourier transform of $U_B(\underline{x})$,

$$\begin{aligned}\hat{U}_B(\underline{k}) &\triangleq \int d\underline{x} e^{-i\underline{k}\cdot\underline{x}} U_B(\underline{x}) \\ &= \int d\underline{\xi}_T \int_0^\infty dr g(\underline{\xi}_T, r) F_2(\underline{k}, r, \underline{\hat{\theta}}, \underline{\xi}) \end{aligned} \tag{C.12}$$

gives (49).

Appendix D

Derivation of equation (52).

From (46), we have

$$\begin{aligned}\hat{g}(\underline{\xi}_T, k_r) &= \int_0^\infty dr e^{-ik_r r} g(\underline{\xi}_T, r) \\ &= \int d\underline{x}' U(\underline{x}') \frac{e^{-ik_r(\hat{\theta}\cdot\underline{x}' + |\underline{x}' - \underline{\xi}|)}}{|\underline{x}' - \underline{\xi}|}. \end{aligned} \tag{D.1}$$

Now taking the Fourier transform with respect to $\underline{\xi}_T$,

$$\begin{aligned}\hat{\hat{g}}(\underline{k}_{\xi T}, k_r) &= \int_{-\infty}^\infty d\underline{\xi}_T e^{-i\underline{k}_{\xi T}\cdot\underline{\xi}_T} \hat{g}(\underline{\xi}_T, k_r) \\ &= \int d\underline{x}' U(\underline{x}') e^{-ik_r\hat{\theta}\cdot\underline{x}'} N(\underline{x}', \underline{k}_{\xi T}, k_r), \end{aligned} \tag{D.2}$$

where

$$N(\underline{x}', \underline{k}_{\xi T}, k_r) = \int d\underline{\xi}_T e^{-i\underline{k}_{\xi T}\cdot\underline{\xi}_T} \frac{e^{-ik_r|\underline{x}' - \underline{\xi}|}}{|\underline{x}' - \underline{\xi}|}. \tag{D.3}$$

To compute $N(\underline{x}', \underline{k}_{\xi T}, k_r)$, we use the polar coordinates $\underline{\xi}_T - \underline{x}'_T = (\rho, \alpha)$, $\underline{k}_{\xi T} = (k_{\xi T}, \beta)$, where $\underline{x}' = (\underline{x}'_T, z')$, so that

$$N(\underline{x}', \underline{k}_{\xi T}, k_r) = 2\pi e^{-i\underline{k}_{\xi T}\cdot\underline{x}'_T} M(z', \underline{k}_{\xi T}, k_r), \tag{D.4}$$

where we have identified

$$\int_0^{2\pi} d\alpha e^{-ik_{\xi T}\rho\cos(\alpha-\beta)} = 2\pi J_0(k_{\xi T}\rho), \tag{D.5}$$

for arbitrary β, and where

$$M(z', \underline{k}_{\xi T}, k_r) \triangleq \int_0^\infty d\rho \rho J_0(k_{\xi T}\rho) \frac{e^{-ik_r\sqrt{\rho^2+z'^2}}}{\sqrt{\rho^2+z'^2}}. \tag{D.6}$$

Now, using the Sommerfeld integral which decomposes a spherical wave into cylindrical waves ([1], Section 6.1),

$$\frac{e^{-ik_r\sqrt{\rho^2+z'^2}}}{\sqrt{\rho^2+z'^2}} = -i\mathrm{sgn}(k_r) \int_0^\infty d\mu \frac{\mu}{\sqrt{k_r^2-\mu^2}} J_0(\mu\rho) e^{-i\mathrm{sgn}(k_r)\sqrt{k_r^2-\mu^2}|z'|}, \tag{D.7}$$

we find that

$$\begin{aligned} M(z', \underline{k}_{\xi T}, k_r) &= -\frac{i\mathrm{sgn}(k_r)}{\sqrt{k_r^2-k_{\xi T}^2}} e^{-i\mathrm{sgn}(k_r)\sqrt{k_r^2-k_{\xi T}^2}|z'|}, \quad \text{for } k_{\xi T} \le |k_r|, \\ &= \frac{1}{\sqrt{k_{\xi T}^2-k_r^2}} e^{-\sqrt{k_{\xi T}^2-k_r^2}|z'|}, \quad \text{for } k_{\xi T} > |k_r|, \end{aligned} \tag{D.8}$$

where we have used the fact that

$$\int_0^\infty d\rho \rho J_0(k_{\xi T}\rho) J_0(\mu\rho) = \frac{1}{\mu}\delta(\mu - k_{\xi T}). \tag{D.9}$$

Substituting $M(z', \underline{k}_{\xi T}, k_r)$ in (D.4) to find $N(\underline{x}', \underline{k}_{\xi T}, k_r)$ and again substituting the resulting $N(\underline{x}', \underline{k}_{\xi T}, k_r)$ in (D.2), we obtain (52).

References

[1] K. Aki and P. G. Richards, *Quantitative Seismology*, Vol. 1, W. H. Freeman & Co., San Francisco, 1980.

[2] G. Beylkin, "Imaging of Discontinuities in the Inverse Scattering Problem by Inversion of a Causal Generalized Radon Transform," *J. Math. Phys.*, Vol. 26, No. 1, pp. 99–108, Jan. 1985.

[3] A. M. Bruckstein, B. C. Levy, and T. Kailath, "Differential Methods in Inverse Scattering," *SIAM J. Appl. Math.*, Vol. 45, No. 2, pp. 312–335, April 1985.

[4] A. J. Berkhout, *Seismic Migration, Imaging of Acoustic Energy by Wave Field Extrapolation, A. Theoretical Aspects*, Elsevier Scientific Publishing Co., 1982.

[5] A. J. Berkhout, *Seismic Migration, Imaging of Acoustic Energy by Wave Field Extrapolation, A. Practical Aspects*, Elsevier Scientific Publishing Co., 1985.

[6] W-F. Chang and G. A. McMechan, "Reverse-Time Migration of Offset Vertical Seismic Profiling Data Using the Excitation-Time Imaging Condition," *Geophysics*, Vol. 51, No. 1, pp. 67–84, Jan. 1986.

[7] J. F. Claerbout, *Imaging the Earth's Interior*, Blackwell Scientific Pub., Oxford, England, 1985.

[8] S. R. Deans, *The Radon Transform and Some of its Applications*, Wiley Interscience, New York, 1983.

[9] A. J. Devaney, "A Filtered Backpropagation Algorithm for Diffraction Tomography," *Ultrasonic Imaging* 4, pp. 336–350, 1982.

[10] A. J. Devaney and G. Beylkin, "Diffraction Tomography Using Arbitrary Transmitter and Receiver Surfaces," *Ultrasonic Imaging* 6, pp. 181–193, 1984.

[11] C. Esmersoy and B. C. Levy, "Multidimensional Born Inversion with a Wide-Band Plane-Wave Source," *Proc. IEEE*, Vol. 74, No. 3, pp. 466–475, March 1986.

[12] C. Esmersoy, M. L. Oristaglio, and B. C. Levy, "Multidimensional Born Velocity Inversion: Single Wideband Point Source," *J. Acoust. Soc. Am.* Vol. 78, No. 3, pp. 1052–1057, Sept. 1985.

[13] J. A. Fawcett, "Inversion of N-Dimensional Spherical Averages," *SIAM J. Appl. Math.*, Vol. 45, No. 2, pp. 336–341, April 1985.

[14] G. H. F. Gardner, editor, *Migration of Seismics Data*, Geophysics Reprint Series, No. 4, Soc. of Explor. Geophysicists, Tulsa, Oklahoma, 1985.

[15] I. S. Gradshteyn and I. M. Ryzhik, *Table of Integrals, Series and Products*, Academic Press, New York, 1980.

[16] M. Kaveh, M. Soumekh, and J. F. Greenleaf, "Signal Processing for Diffraction Tomography," *IEEE Trans. Sonics Ultrasonics*, Vol. SU-31, No. 4, pp. 230–239, July 1984.

[17] D. Miller, M. Oristaglio, and G. Beylkin, "A New Slant on Seismic Imaging: Classical Migration and Integral Geometry," Research Note, Schlumberger-Doll Research, Jan. 1986.

[18] P. M. Morse and H. Feshbach, *Methods of Theoretical Physics*, Part 1, McGraw-Hill, New York, 1953.

[19] R. K. Mueller, M. Kaveh, and R. D. Iverson, "A New Approach to Acoustic Tomography Using Diffraction Techniques," in *Acoustic Imaging Vol. 8*, A. F. Metherell, ed. pp. 615–628, Plenum Press, New York, 1980.

[20] J. Radon, "Über die Bestimmung von Funktionen durch ihre Integralwerte längs gewisser Mannigfaltigkeiten," *Berichte Sächsische Akademie der Wissenschaften. Leipzig, Math.-Phys. Kl.* 69, pp. 262–267, 1917.

[21] B. A. Roberts and A. C. Kak, "Reflection Mode Diffraction Tomography," *Ultrasonic Imaging* 7, pp. 300–320, 1985.

[22] M. Soumekh, "Image Reconstruction Techniques in Tomographic Imaging Systems," *IEEE Trans. Acoust. Speech Signal Processing*, Vol. ASSP-34, No. 4, Aug. 1986.

[23] A. Tarantola, "Linearized Inversion of Seismic Reflection Data," *Geophysical Prospecting*, Vol. 32, pp. 998–1015, 1984.

[24] J. R. Taylor, *Scattering Theory*, John Wiley, New York, 1972.

Figure Captions

Fig. 1 2-D experimental geometry.

Fig. 2 Generalized parabolic projections.

Fig. 3 Coverage of $\hat{U}(\underline{k})$ for a single array.

Fig. 4 Scattering potential for the synthetic experiment.

Fig. 5 Reconstruction using the receivers on Side A.

Fig. 6 Reconstruction using the receivers on Side B.

Fig. 7 Reconstruction using the receivers on Side C.

Fig. 8 Reconstruction using all the receivers.

Fig. 9 Coverage of $\hat{U}(\underline{k})$ due to receivers on Side A. Lightly shaded regions indicate the coverage for the case of an infinite bandwidth source; the darkly shaded regions mark the coverage for a finite bandwidth source.

Fig. 10 Coverage of $\hat{U}(\underline{k})$ due to receivers on Side B. Lightly shaded regions indicate the coverage for the case of an infinite bandwidth source; the darkly shaded regions mark the coverage for a finite bandwidth source.

Fig. 11 Coverage of $\hat{U}(\underline{k})$ due to receivers on Side C. Lightly shaded regions indicate the coverage for the case of an infinite bandwidth source; the darkly shaded regions mark the coverage for a finite bandwidth source.

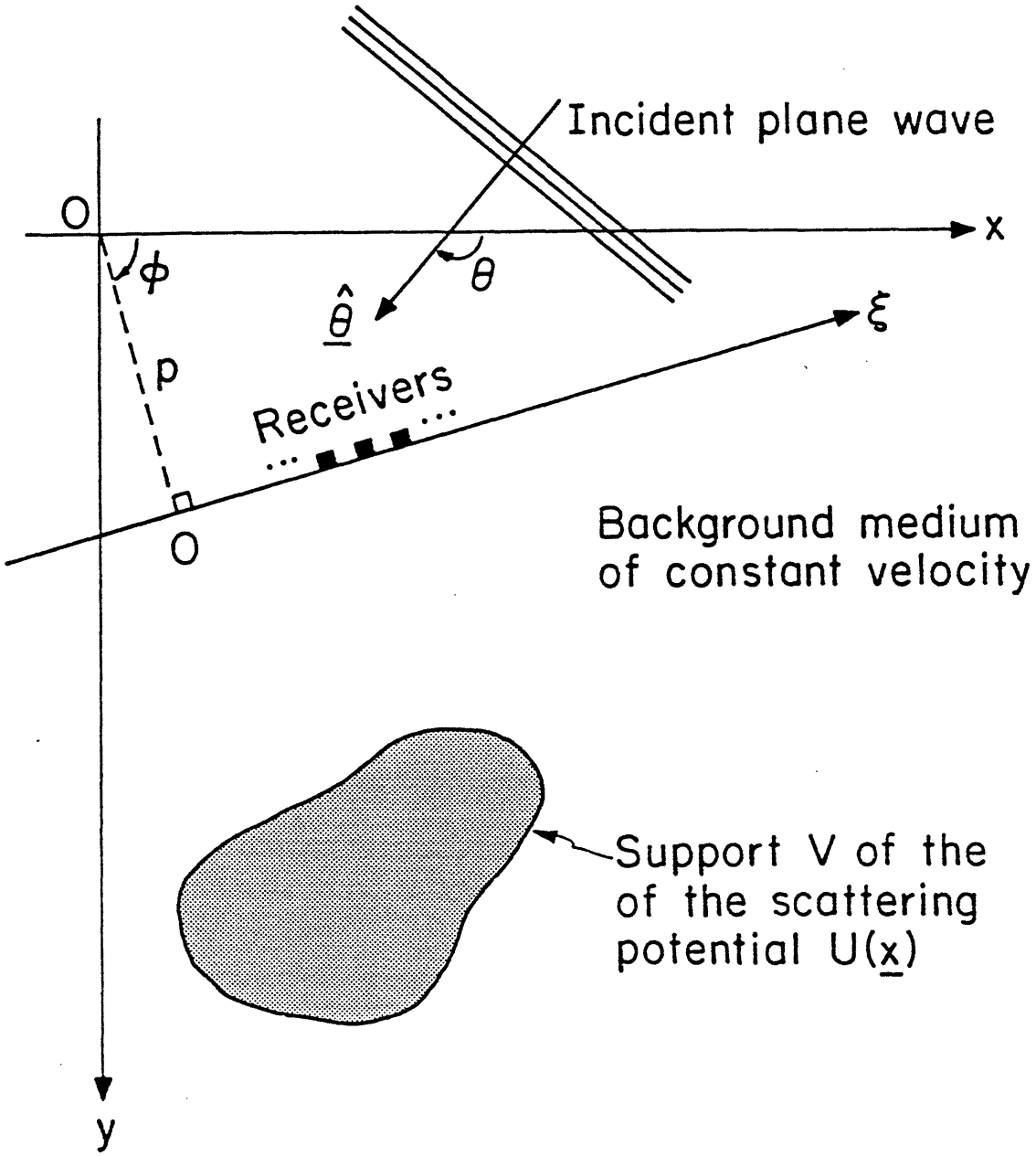
Incident plane wave
O
x
ϕ
θ
$\hat{\theta}$
ξ
p
Receivers
O
Background medium
of constant velocity
Support V of the
of the scattering
potential U(x)
y

FIG. 1

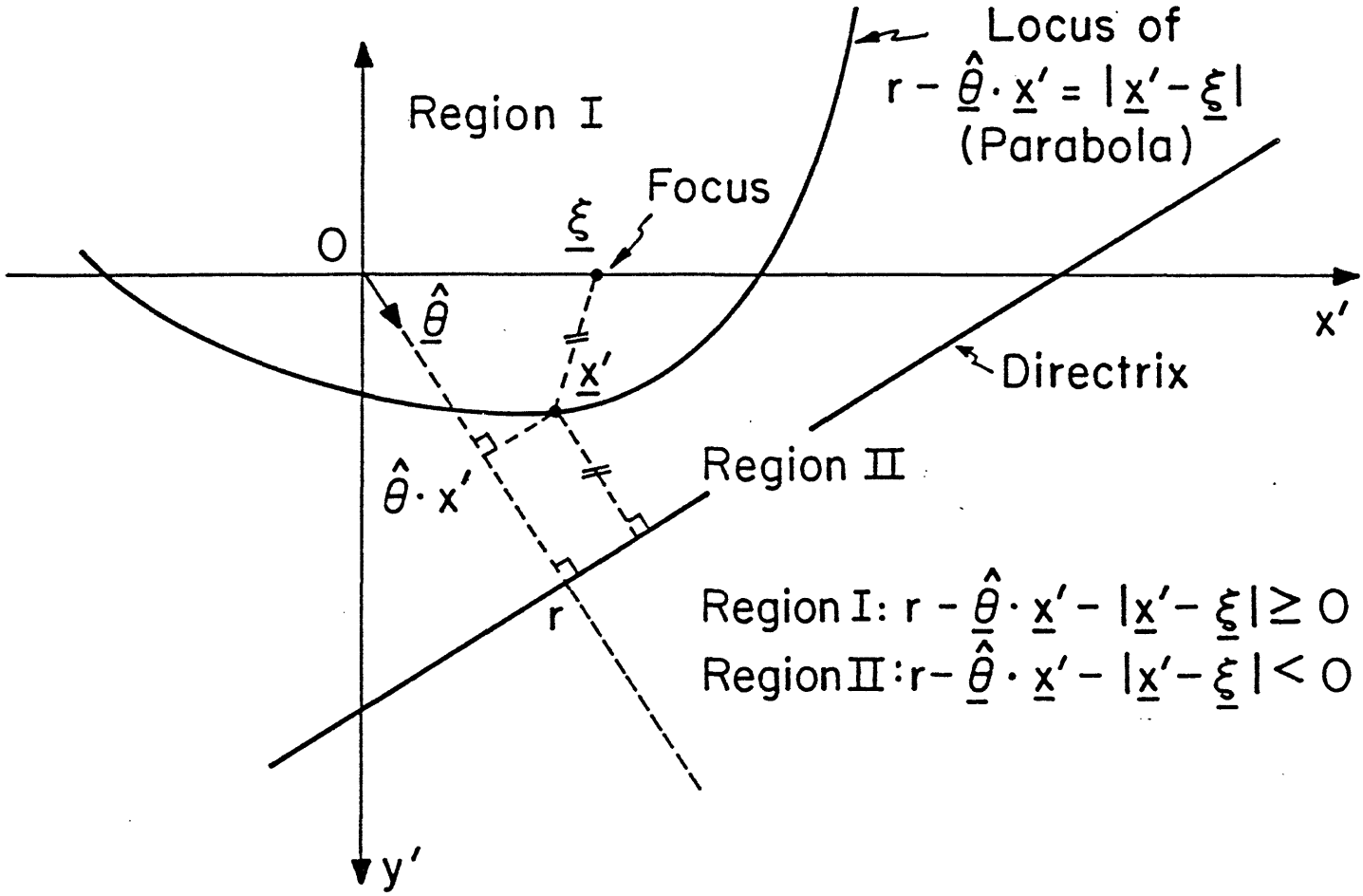
Locus of
$r - \hat{\theta} \cdot \underline{x}' = |\underline{x}' - \underline{\xi}|$
(Parabola)
Region I
Focus
$\underline{\xi}$
O
$\hat{\theta}$
$\underline{x}'$
x'
Directrix
Region II
$\hat{\theta} \cdot x'$
r
Region I: $r - \hat{\theta} \cdot \underline{x}' - |\underline{x}' - \underline{\xi}| \geq 0$
Region II: $r - \hat{\theta} \cdot \underline{x}' - |\underline{x}' - \underline{\xi}| < 0$
y'

FIG. 2

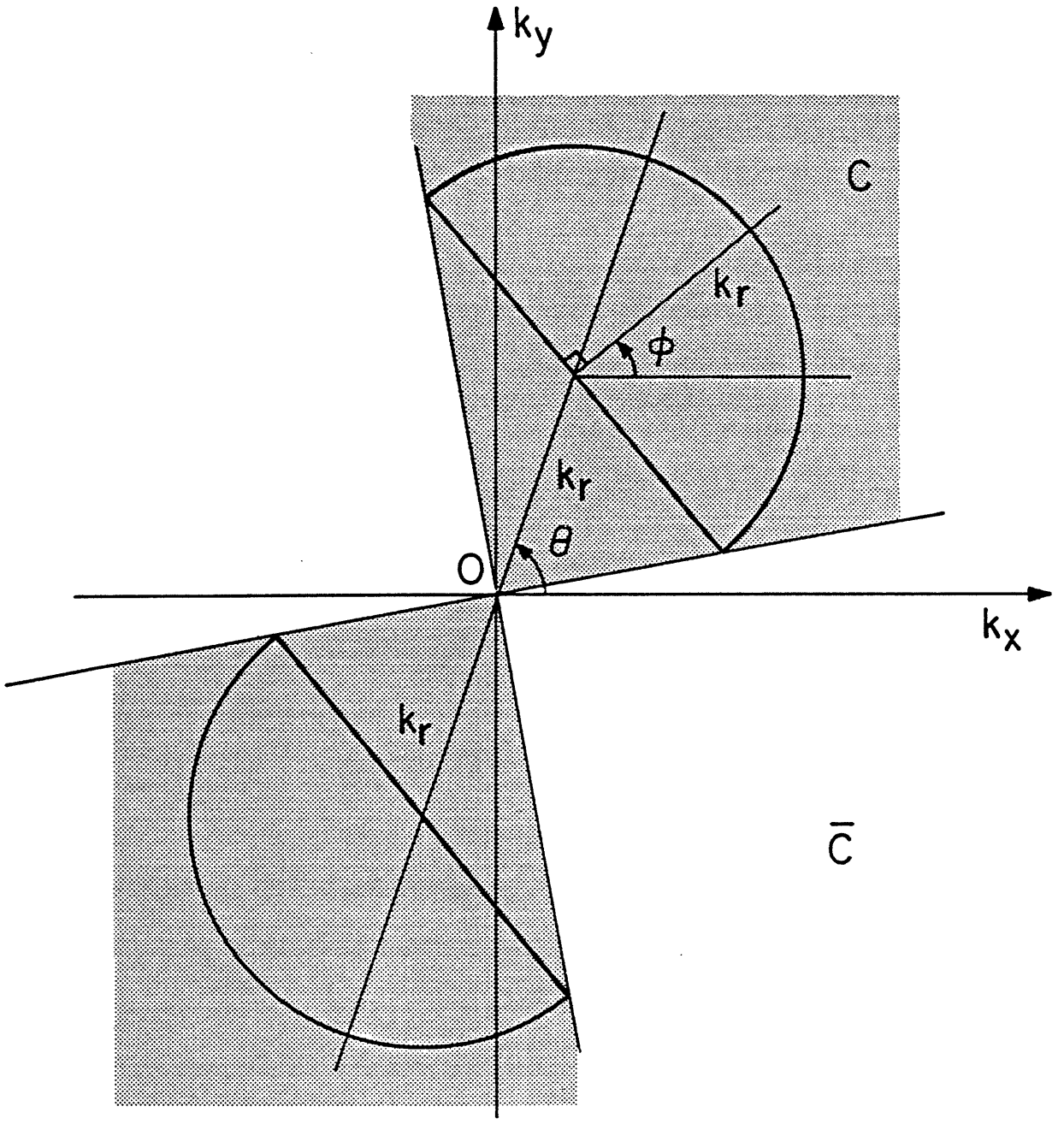

FIG. 3

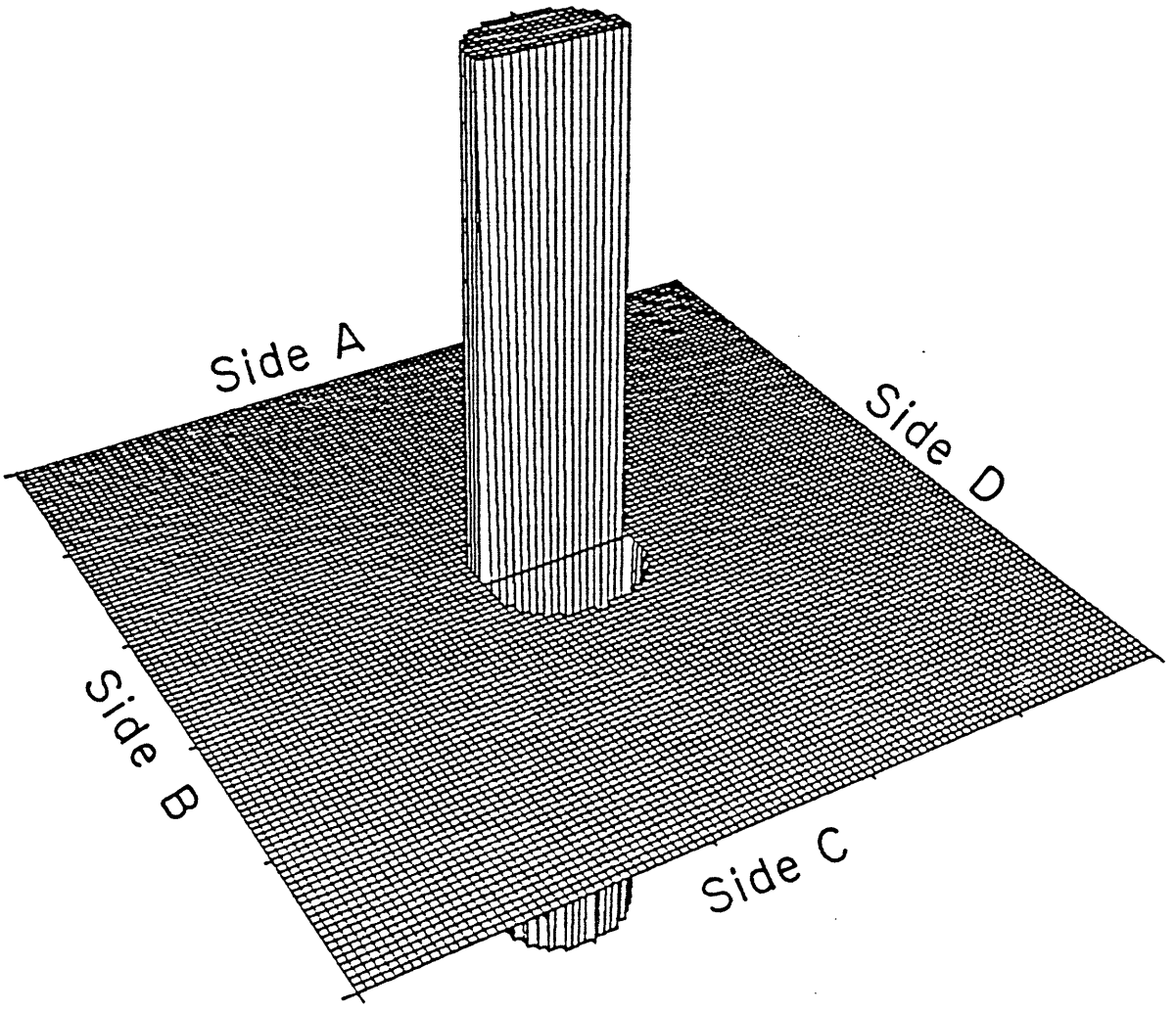

FIG. 4

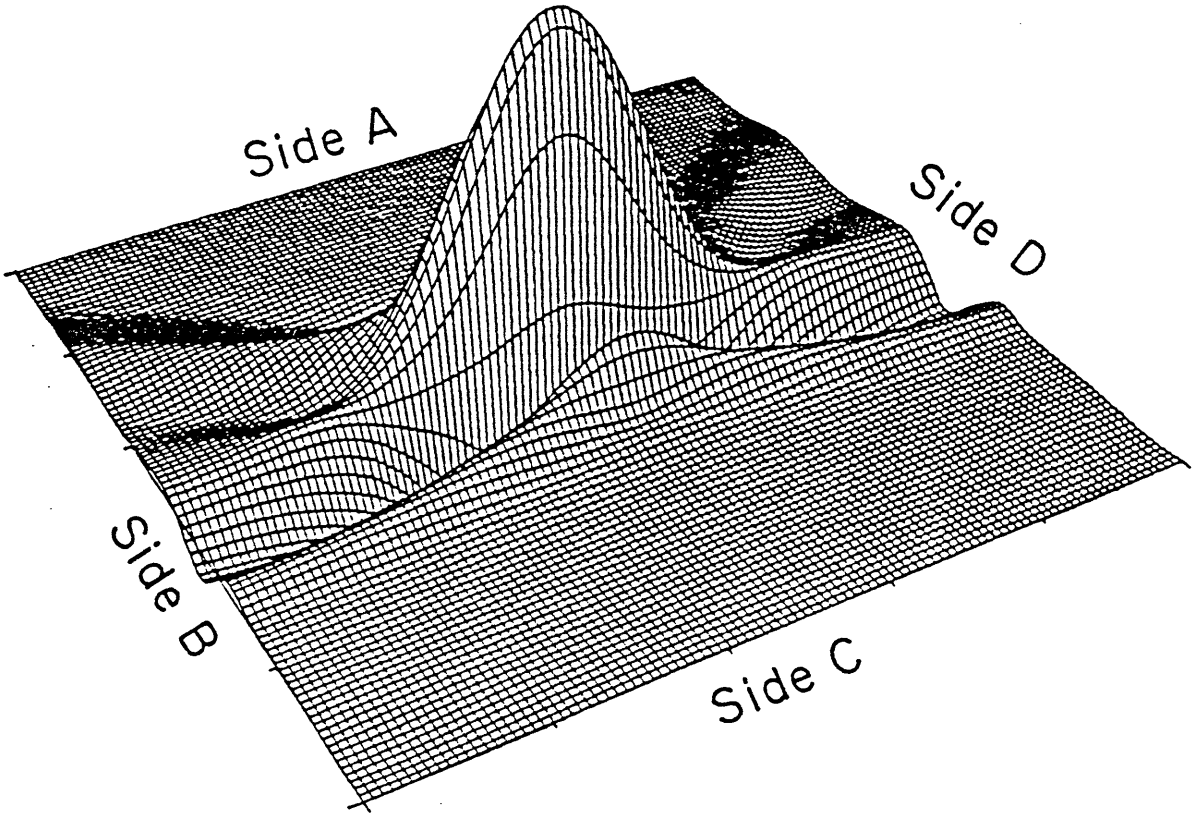

FIG. 5

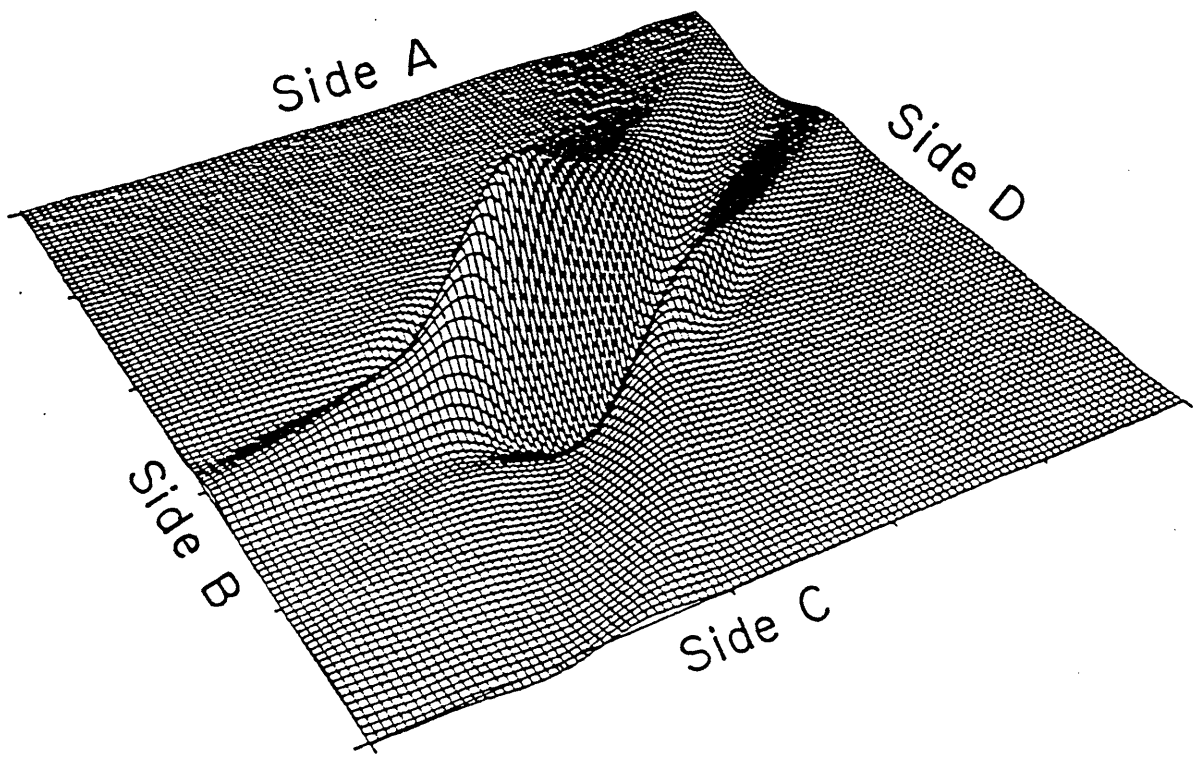

FIG. 6

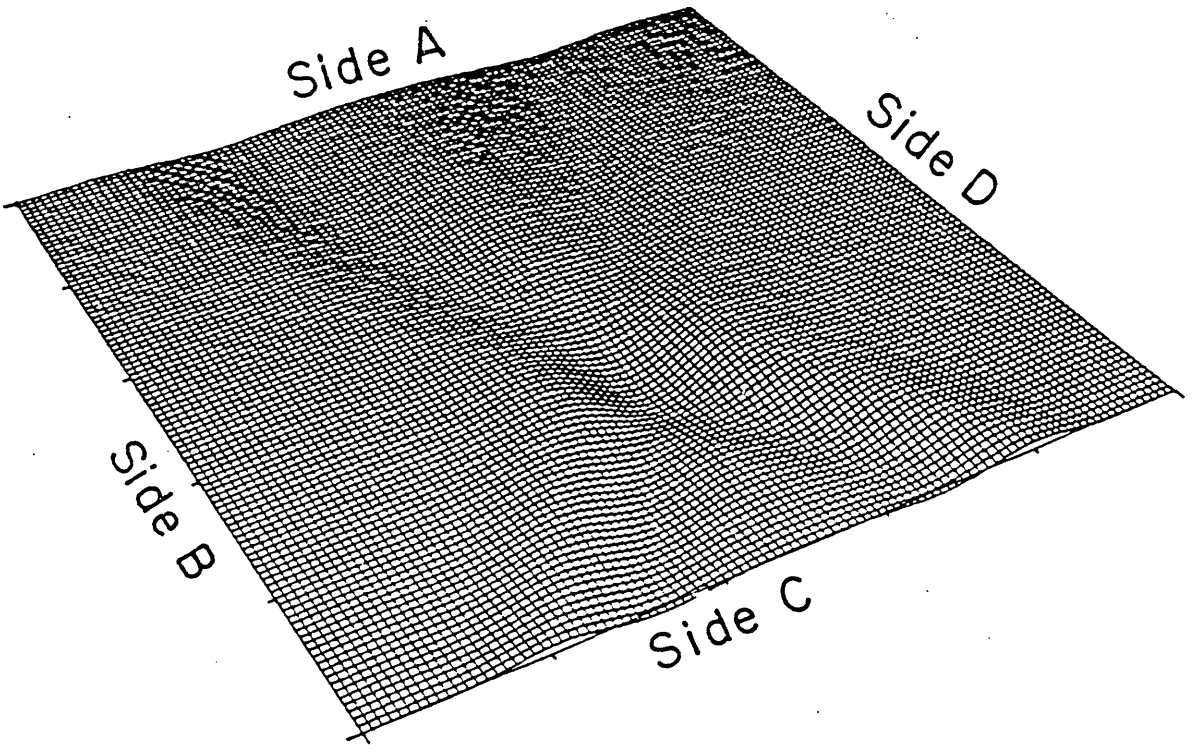

FIG. 7

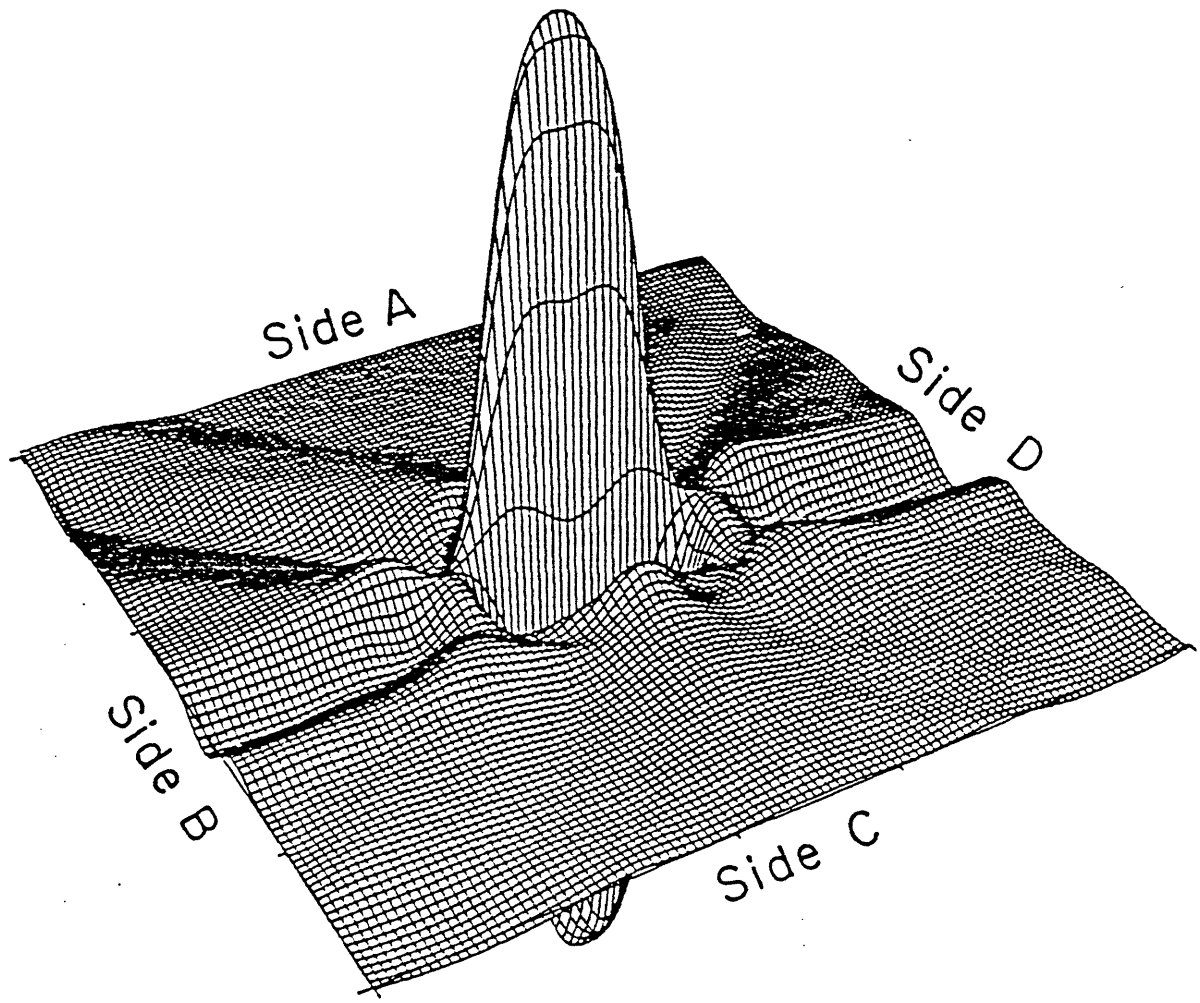

FIG. 8

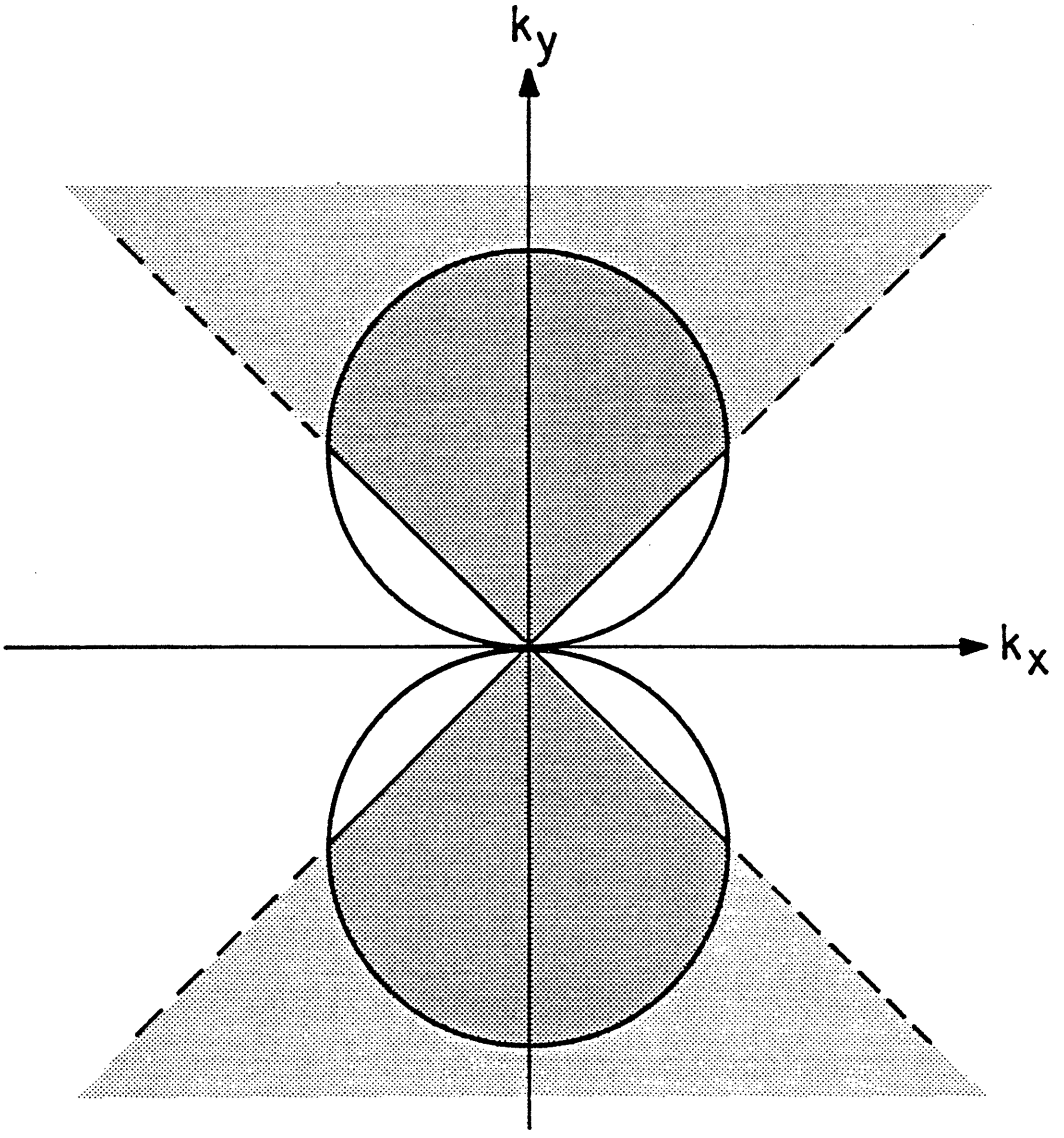

FIG. 9

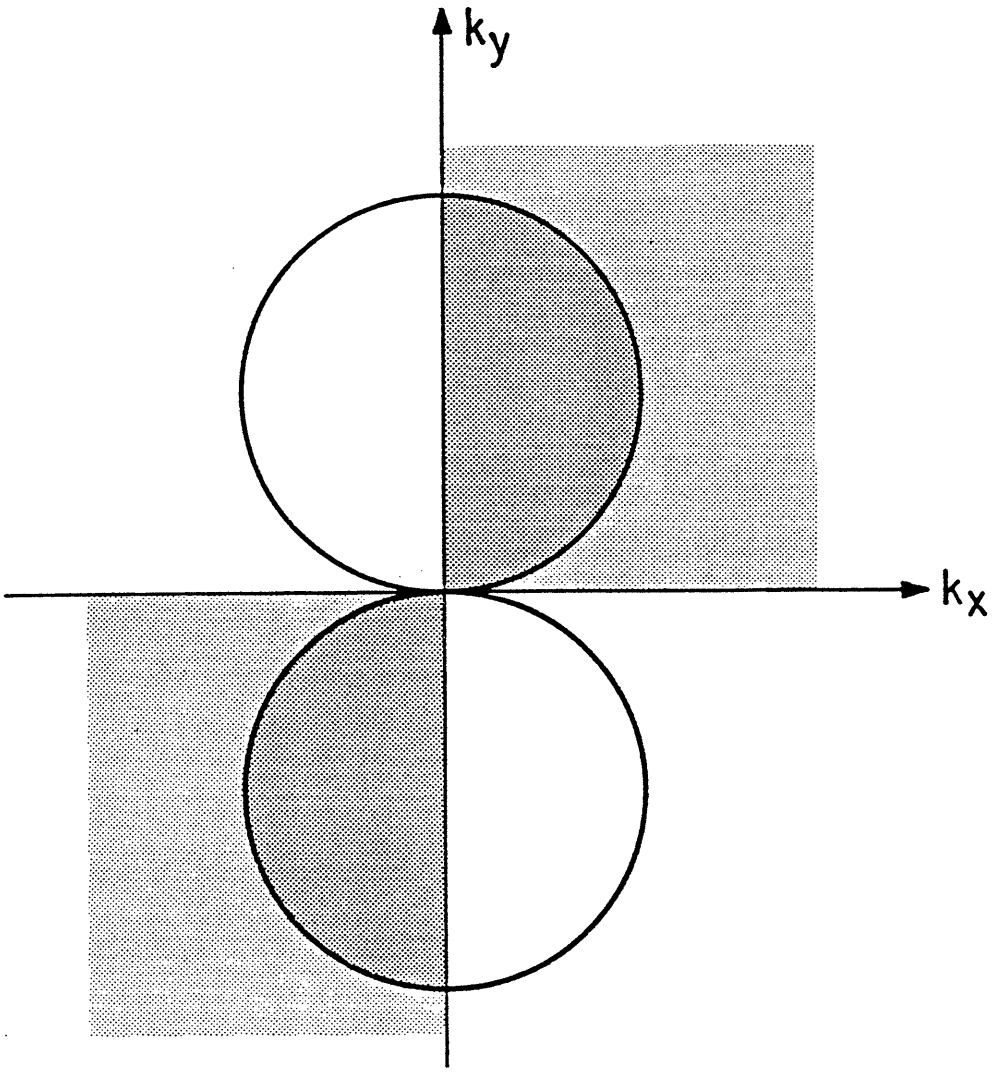

FIG. 10

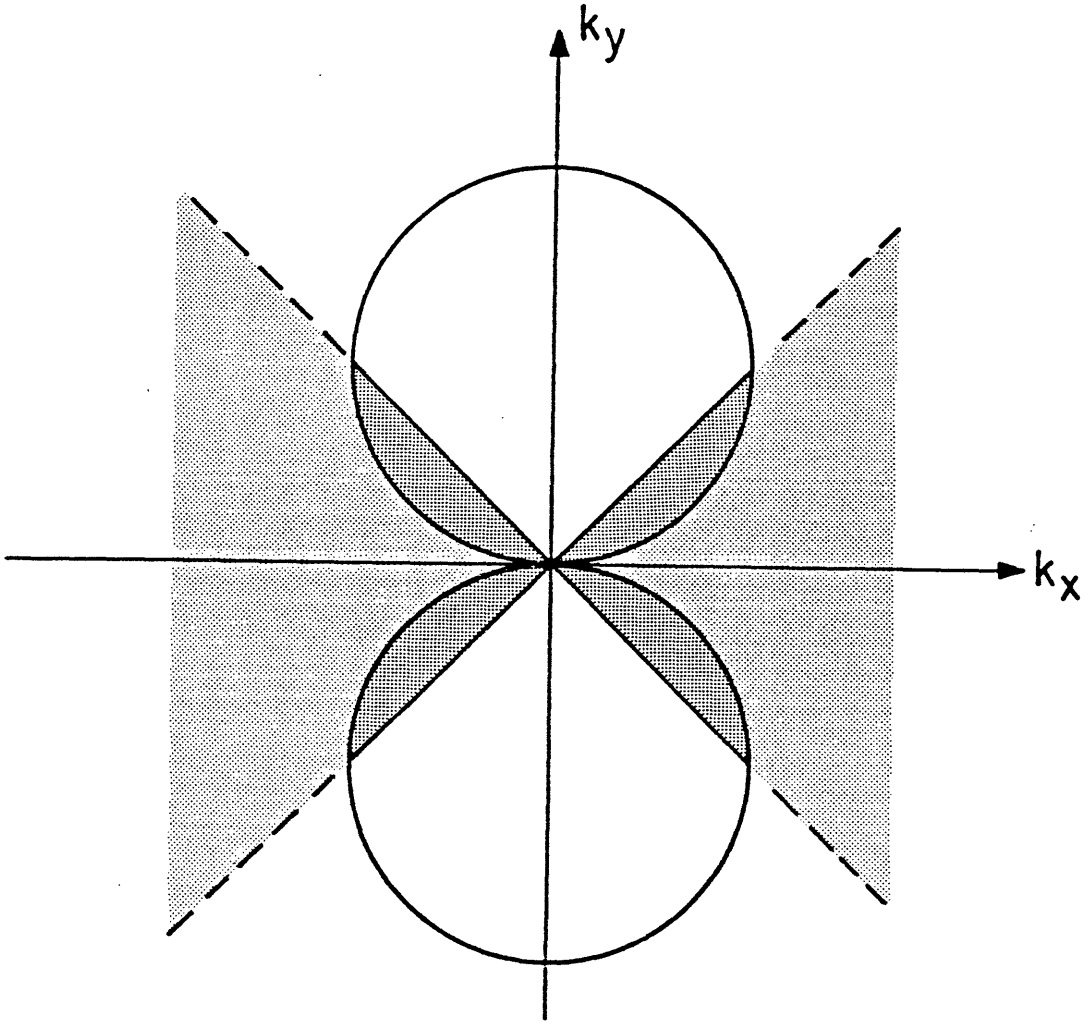

FIG. 11